Supporting Information For:

A Mechanistic Study on the Solution Phase N-Doping of 1,3-Dimethyl-2-Aryl-2,3-Dihydro-1H-Benzoimidazole Derivatives

By Benjamin D. Naab,[§] Song Guo,[≈] Selina Olthof,[ϟ] Eric G.B. Evans,[‡] Peng Wei,[§] Glenn L. Millhauser,[‡] Antoine Kahn,[ϟ] Stephen Barlow,[,†] Seth Marder,*[,†] and Zhenan Bao*[,§]*

[§]Department of Chemical Engineering, and Department of Chemistry
Stanford University, 359 N-S Axis Stauffer III, Stanford, CA 94303 U.S.
*Address Correspondence To: zbao@stanford.edu

[†]School of Chemistry and Biochemistry and Center for Organic Photonics and Electronics
Georgia Institute of Technology, 901 Atlantic Drive, Atlanta, GA 30332 U.S.
*Address Correspondence To: seth.marder@chemistry.gatech.edu, stephen.barlow@chemistry.gatech.edu

[≈]Department of Chemistry and Biochemistry
The University of Southern Mississippi, Hattiesburg, MS 39406

[ϟ]Department of Electrical Engineering
Princeton University, B420 Engineering Quadrangle, Princeton, NJ 08544
*Address Correspondence To: kahn@princeton.edu

[‡]Department of Chemistry and Biochemistry
University of California – Santa Cruz, 1156 High Street, Santa Cruz, CA 95064
*Address Correspondence To: glennm@ucsc.edu

General Methods:

Chemicals were obtained from commercial sources and used as received unless stated otherwise. Reagent grade chlorobenzene and acetonitrile was passed through an alumina column, refluxed over P_2O_3, distilled and deoxygenated by the freeze-pump-thaw method prior to use. ^{1}H-NMR and ^{13}C-NMR spectra were recorded in D_6-DMSO, or D_6-Acetone on Varian 400 MHz or 300MHz NMR spectrometers. The chemical shifts (δ) are reported in parts per million (ppm). Electrospray ionization mass spectrometry (ESI-MS), direct analysis in real time mass spectrometry (DART-TOF-MS), and matrix assisted laser desorption ionization MALDI-TOF-MS were performed at the University of Florida mass spectrometry facilities. Additionally, some ESI-MS for the $PC_{61}BM$:N-DMBI aggregates was performed at the University of Washington mass spectrometry facilities. Elemental analysis was performed by Robertson Microlit.

Synthesis:

Preparation of α-deutero-dimethylaminobenzaldehyde. A small dry argon flushed vial was charged with deuterated dimethylformamide (260 µL, 3.3 mmol) then cooled to 0 ºC. To this phosphoryl chloride (150 µL, 1.65 mmol) was slowly added drop wise after which the solution was warmed to room temperature (RT). Dimethylaniline (210 µL, 1.65 mmol) was then added, and the solution was heated to 90 ºC for 2 h with stirring under argon. The reaction mixture was then diluted with ice and neutralized to pH of 6-8 with 10 wt% aqueous sodium acetate solution. The solids that formed were collected by vacuum filtration and washed with water until the color cleared. The crude product was stored under argon at -20ºC, and used without further purification.

General procedure for preparation of benzimidazoles. A 20 ml vial was charged with *N, N'*-dimethyl-*o*-phenylenediamine (136 mg, 1.00 mmol) in methanol (2 mL) to this was added the appropriate aromatic aldehyde (1.00 mmol). One drop of glacial acetic acid was then added, and the solution was sonicated at room temperature until precipitation was observed. The crude product was then collected by vacuum filtration, and recrystallized from methanol/H_2O to give the corresponding pure 1,3-dimethyl-2-arylbenzimidazoles.

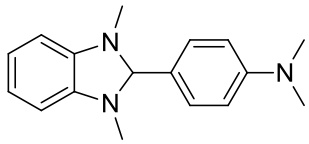

^{1}H NMR (D_6-DMSO, 300 MHz): 7.34 (d, 2H), 6.75 (d, 2H), 6.58 (dd, 2H), 6.42 (dd, 2H), 4.71 (s, 1H), 2.93 (s, 6H), 2.44 (s, 6H); ^{13}C{^{1}H} NMR (D_6-DMSO, 300MHz): 151.28, 142.25, 129.57, 125.47, 119.09, 112.14, 105.82, 93.46, 40.27, 33.09; ESI-MS = 266.1659 ($M-H^+$), 268.1811 ($M+H^+$)

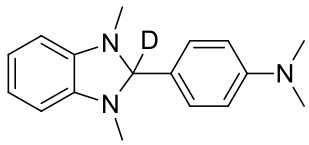

^{1}H NMR (D_6-DMSO, 300 MHz): 7.34 (d, 2H), 6.76 (d, 2H), 6.59 (dd, 2H), 6.41 (dd, 2H), 2.93 (s, 6H), 2.44 (s, 6H); ^{13}C{^{1}H} NMR (D_6-DMSO, 300MHz): 150.98, 142.00, 129.23, 125.16, 118.72, 111.84, 105.47, (*C*D imidazole resonance not observed), 39.993, 32.78; ESI-MS = 266.1659 ($M-D^+$), 269.1880 ($M+H^+$)

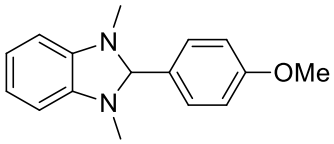

^{1}H NMR (D_6-DMSO, 300 MHz): 7.46 (d, 2H), 7.00 (d, 2H), 6.61 (dd, 2H), 6.44 (dd, 2H), 4.79 (s, 1H), 3.78 (s, 3H), 2.45 (s, 6H); ^{13}C{^{1}H} NMR (D_6-DMSO, 300 MHz): 159.98, 141.93, 130.47, 129.84, 118.97, 113.81, 105.71, 92.85, 55.13, 32.96; ESI-MS = 253.1331 ($M\text{-}H^+$)

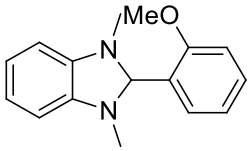

^{1}H NMR (D_6-DMSO, 300 MHz): 7.65 (dd, 1H), 7.37 (td, 1H), 7.12 (d, 1H), 7.03 (t, 1H), 6.59 (dd, 2H), 6.41 (dd, 2H), 5.47 (s, 1H), 3.82 (s, 3H), 2.48 (s, 6H); ^{13}C{^{1}H} NMR (D_6-DMSO, 300 MHz): 158.65, 142.1, 130.01, 128.73, 126.23, 120.79, 118.88, 111.27, 105.61, 84.65, 55.66, 33.19; ESI-MS = 253.1335 ($M\text{-}H^+$), 255.1491 ($M+H^+$)

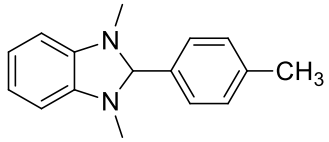

^{1}H NMR (D_6-DMSO, 300 MHz): 7.43 (d, 2H), 7.25 (d, 2H), 6.62 (dd, 2H), 6.45 (dd, 2H), 4.81 (s, 1H), 2.46 (s, 6H), 2.34 (s, 3H); ^{13}C{^{1}H} NMR (D_6-DMSO, 300 MHz): 141.94, 138.63, 135.76, 129.06, 128.57, 118.99, 105.72, 93.06, 33.01, 20.89; ESI-MS = 237.1380 ($M\text{-}H^+$)

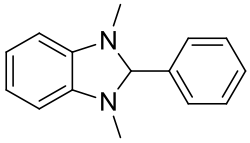

^{1}H NMR (D_6-DMSO, 300 MHz): 7.6-7.4 (m, 5H), 6.62 (dd, 2H), 6.47 (dd, 2H), 4.87 (s, 1H), 2.48 (s, 6H); ^{13}C{^{1}H} NMR (D_6-DMSO): 141.91, 138.74, 129.27, 128.62, 128.45, 119.04, 105.76, 93.21, 33.06; ESI-MS = 223.1233 ($M\text{-}H^+$)

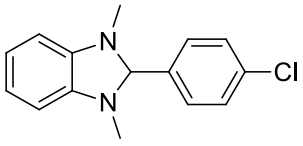

^{1}H NMR (D_6-DMSO, 300 MHz): 7.57 (m, 2H), 7.50 (m, 2H), 6.72 (dd, 2H), 6.46 (dd, 2H), 4.89 (s, 1H), 2.47 (s, 6H); ^{13}C{^{1}H} NMR (D_6-DMSO, 300MHz): 141.80, 137.92, 133.77, 130.46, 128.54, 119.14, 105.87, 92.31, 33.09; ESI-MS = 257.0833 ($M\text{-}H^+$)

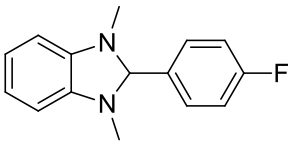

^{1}H NMR (D_6-DMSO, 300 MHz): 7.60 (t, 2H), 7.28 (t, 2H), 6.62 (dd, 2H), 6.45 (dd, 2H), 4.88 (s, 1H), 2.47 (s, 6H); ^{13}C{^{1}H} NMR (D_6-DMSO, 300 MHz): 162.63 (d, J_{CF} = 244.9 Hz), 141.81, 135.03, 130.65 (d, J_{CF} = 8.4 Hz), 119.10, 115.32 (d, J_{CF} = 21.4 Hz), 105.82, 92.36, 33.03; ESI-MS = 241.1139 (M-H^{+})

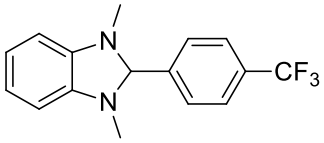

^{1}H NMR (D_6-Acetone, 400 MHz): 7.82 (m, 4H), 6.67 (dd, 2H), 6.48 (dd, 2H), 4.99 (s, 1H), 2.56 (s, 6H); ^{13}C{^{1}H} NMR (D_6-Acetone, 400 MHz): 145.72, 143.01, 131.65 (q, J_{CF} = 32.0 Hz), 130.56, 126.25 (q, J_{CF} = 3.8 Hz), 125.35 (q, J_{CF} = 271.6 Hz), 120.37, 106.88, 94.14, 33.67; ESI-MS = 291.1097 (M-H^{+})

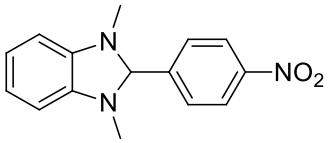

^{1}H NMR (D_6-DMSO, 300 MHz): 8.31 (m, 2H), 7.85 (m, 2H), 6.66 (dd, 2H), 6.51 (dd, 2H), 5.09 (s, 1H), 2.52 (s, 6H); ^{13}C{^{1}H} NMR (D_6-DMSO, 300MHz): 148.19, 147.37, 141.70, 129.97, 123.68, 119.33, 106.05, 91.85, 33.25; ESI-MS = 268.1071 (M-H^{+})

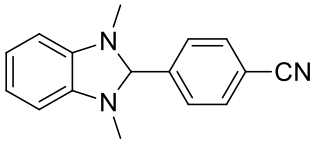

^{1}H NMR (D_6-DMSO, 300 MHz): 7.94 (m, 2H), 7.76 (m, 2H), 6.65 (dd, 2H), 6.49 (dd, 2H), 5.02 (s, 1H), 2.50 (s, 6H); ^{13}C{^{1}H} NMR (D_6-DMSO, 300MHz): 144.47, 141.72, 132.53, 129.62, 119.28, 118.65, 112.03, 106.01, 92.23, 33.22; ESI-MS = 248.1170 (M-H^{+})

ESR Detection Experiments. The EPR measurements were performed on an X-band Bruker EMX operating 9.44 GHz with a Bruker SHQ cavity with variable temperature control. The EPR spectra were recorded under non-saturating microwave power conditions. The magnitude of modulation was chosen to optimize the resolution and the signal-to-noise (S/N) ratio of the observed spectra. The *g*-values were calibrated against an external DPPH standard. Spin quantification experiments were performed on thin-films of doped C_{60} prepared by evaporation of toluene solutions on the walls of the EPR tube. Double integrals of the spectra were compared to external TEMPO standards in toluene.

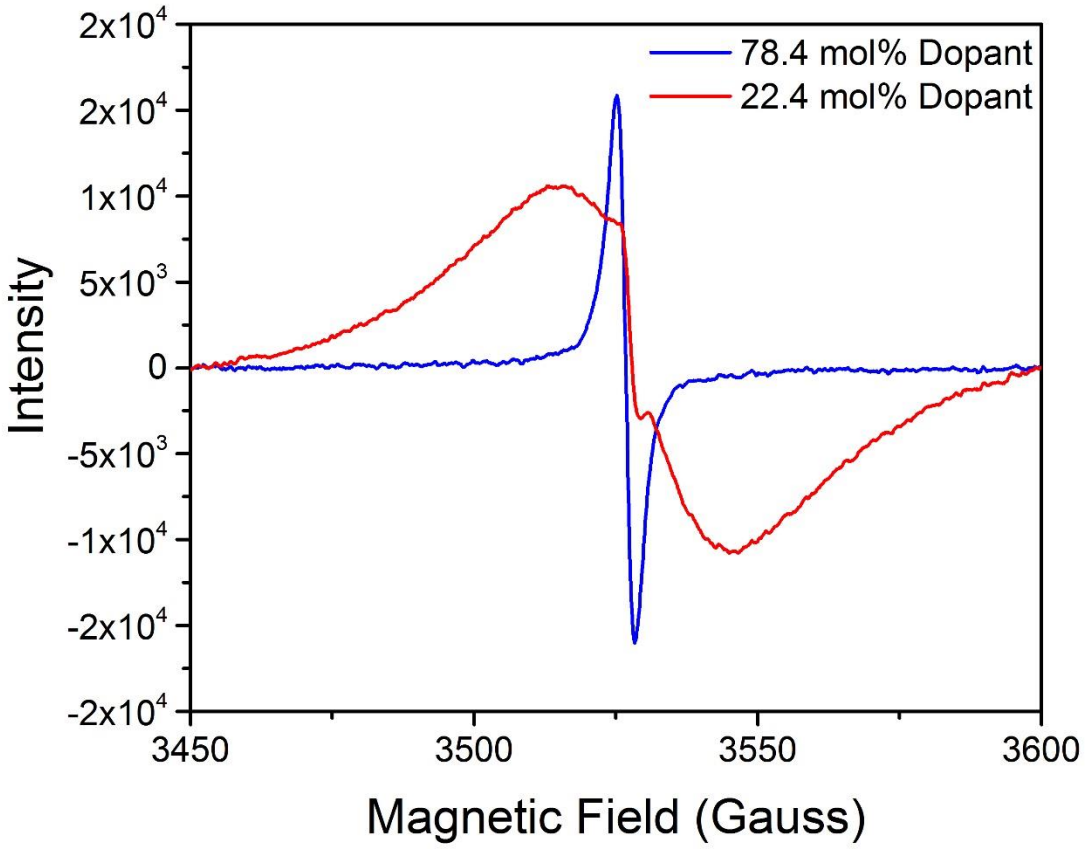

Figure S1: Evolution of *o*-MeO-DMBI doped C_{60} peak shape for two samples with different C_{60} masses with equivalent dopant masses present in the two films. (high conc. = 78.4 mol%, low conc. = 22.4 mol%).

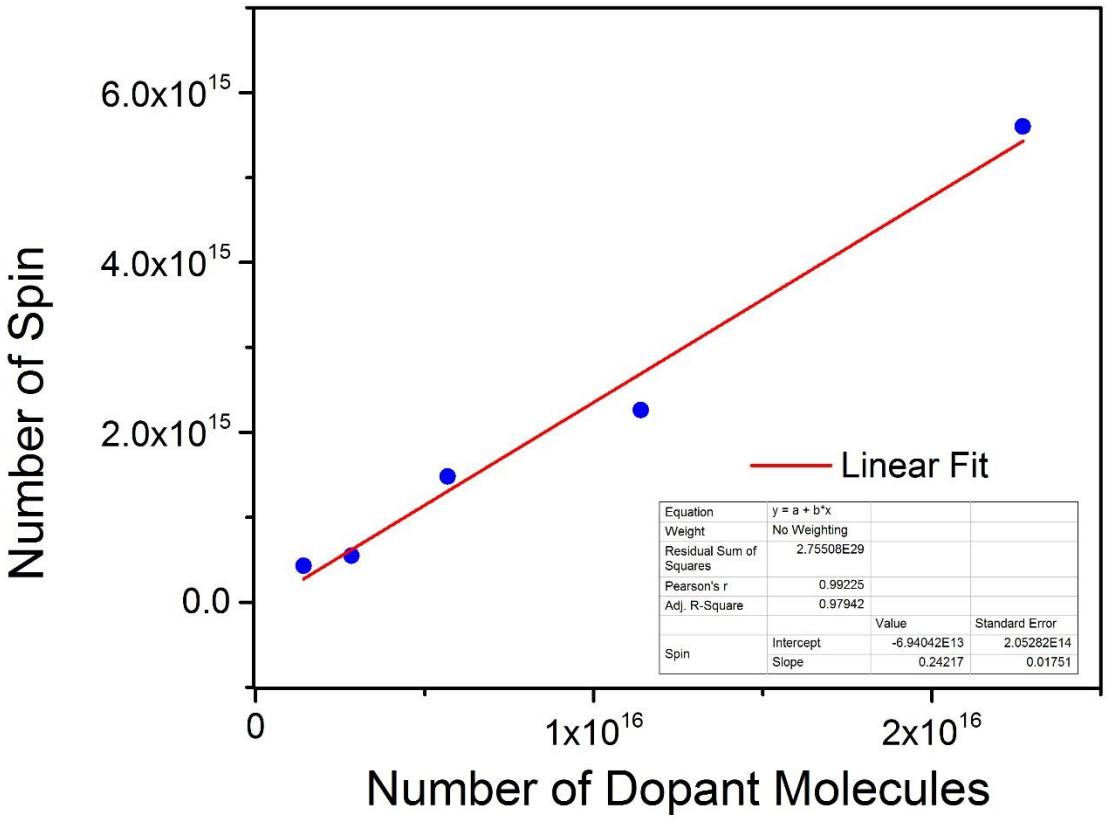

Figure S2: Quantitative ESR data for *o*-MeO-DMBI doped C_{60} thin-films at various doping concentrations. At concentrations >20 mol% a deviation from linearity is observed, but the spin-density rises very linearly with the dopant density at lower doping concentrations.

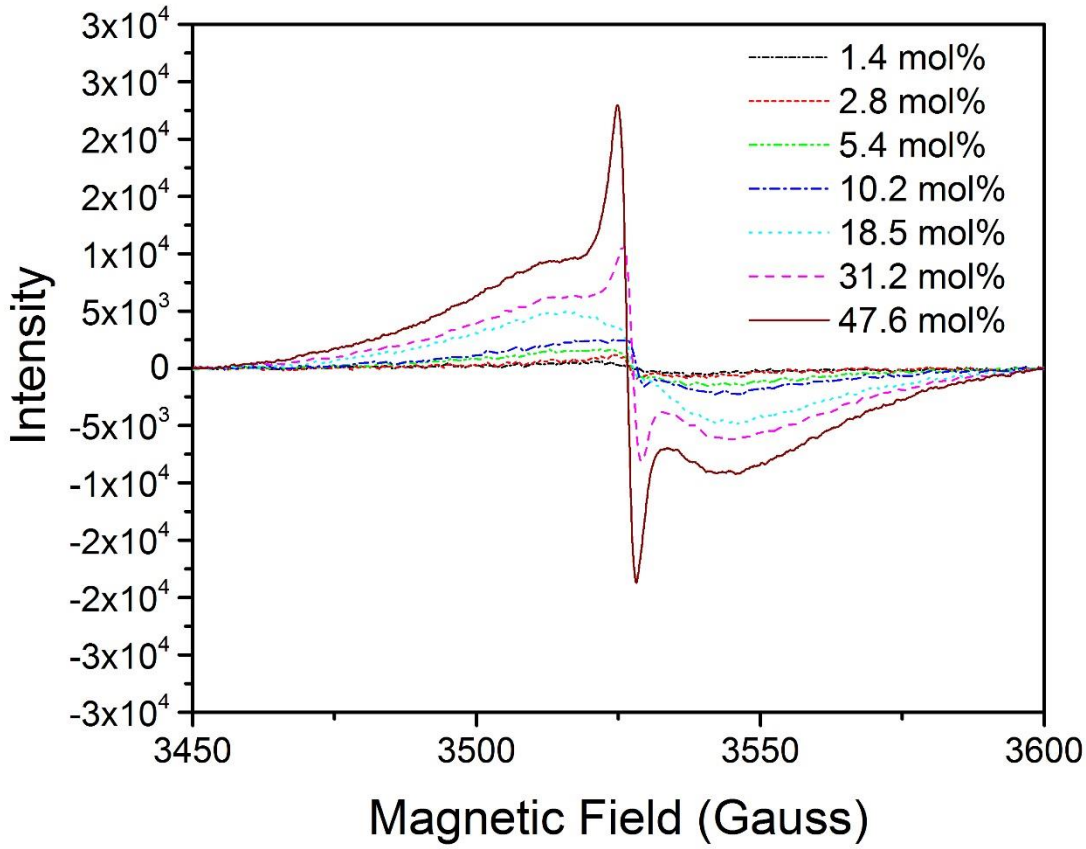

Figure S3: ESR spectra for *o*-MeO-DMBI doped C_{60} thin-films at various doping concentrations.

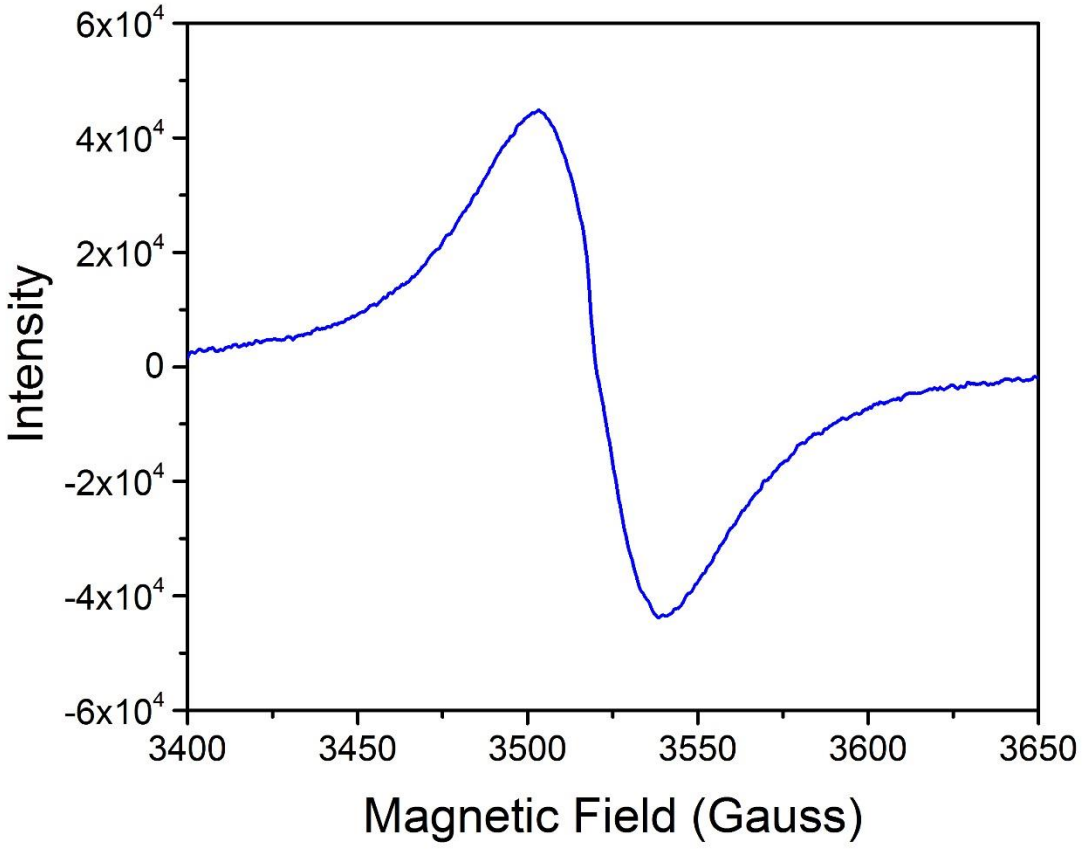

Figure S4: ESR spectrum of a sample of the isolated precipitate of *o*-MeO-DMBI and C_{60}.

Ultraviolet/Visible/Near-Infrared (UV-Vis-NIR) Spectroscopy measurements:

The samples for UV-vis-NIR measurements were prepared in a glove-box and then transferred into polytetrafluoroethylene (PTFE) stopcock-sealed quartz cuvettes (175–2700 nm) with path lengths of 1 mm. The cuvettes were then taken to a Varian Cary 5E ultraviolet-visible-near infrared spectrometer to monitor the reaction progress. A Quantum Northwest TC 125 temperature controller was used to control the temperature of the sample cuvette holder.

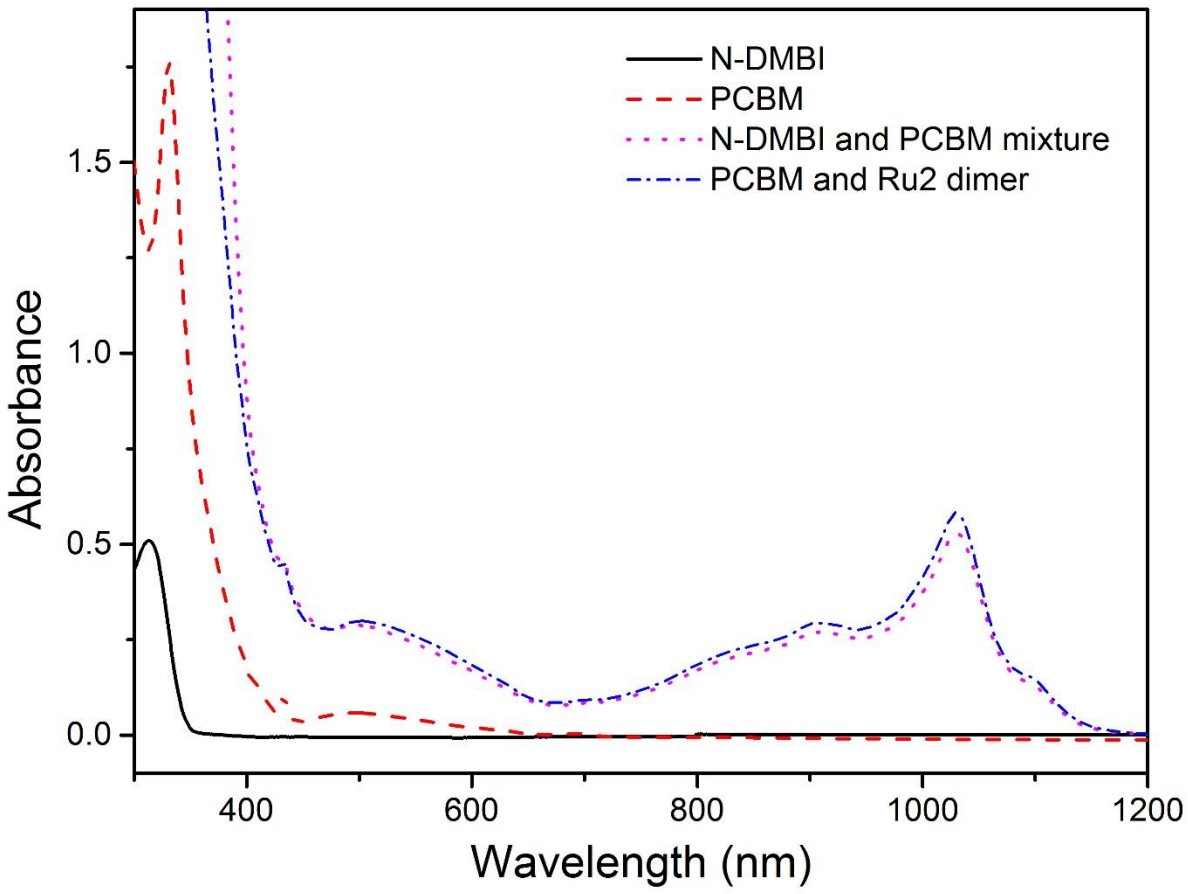

Figure S5: UV-Vis-NIR comparison of $PC_{61}BM$, N-DMBI, and mixtures of $PC_{61}BM$ with $[Ru(Cp^*)(TEB)]_2$ and N-DMBI. The spectra for the two mixtures are near perfect matches in the NIR indicating a common absorption that is assigned to the $PC_{61}BM$ radical anion. [N-DMBI] = 4.8 x 10^-4 M, [PCBM} = 2.2 x 10^-4 M, The mixture: [N-DMBI] = 2.4 x 10^-4 M, [PCBM} = 5.5 x 10^-4 M.

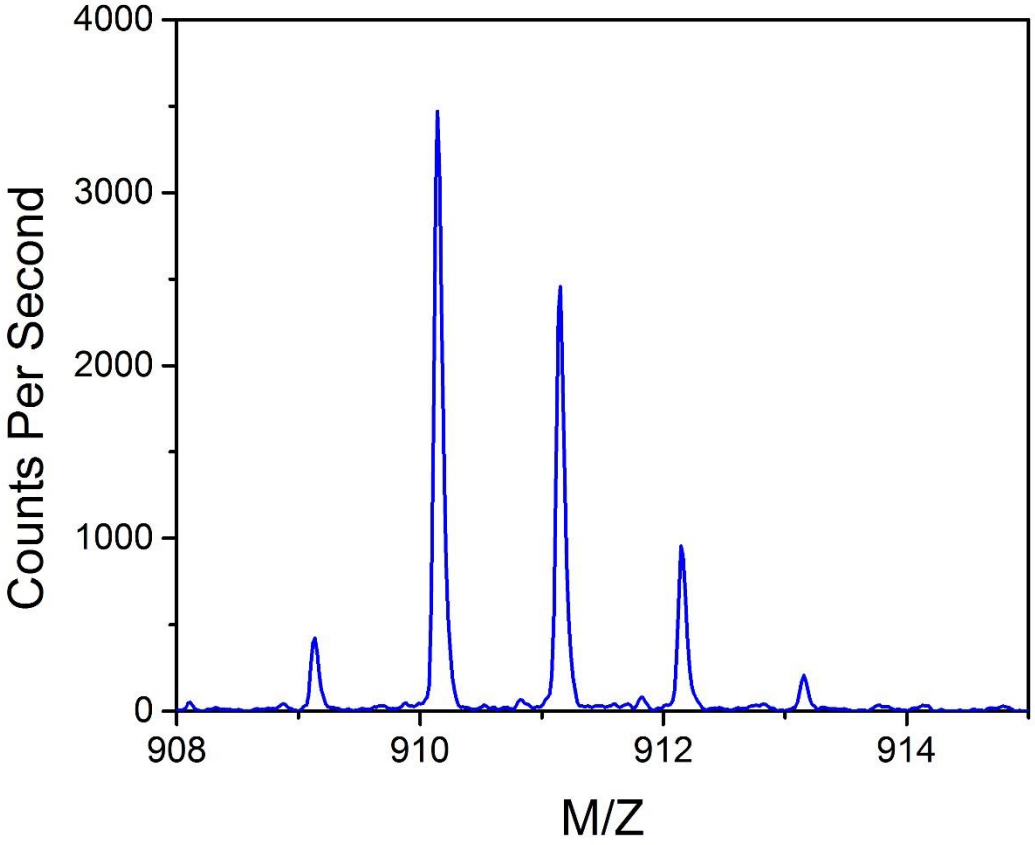

Figure S6: The DART-TOF-MS spectra for the $PC_{61}BM$ molecular ion.

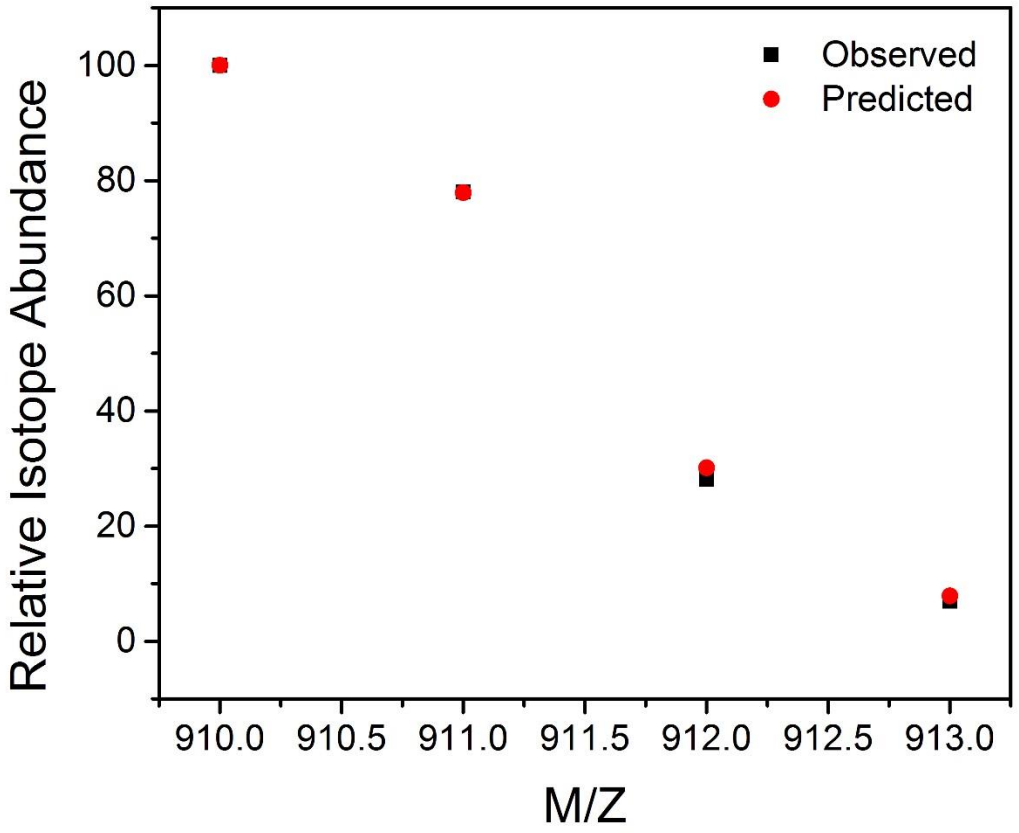

Figure S7: Comparison of predicted and observed relative isotope abundance for $PC_{61}BM$. The observed spectra were recorded using DART-TOF-MS.

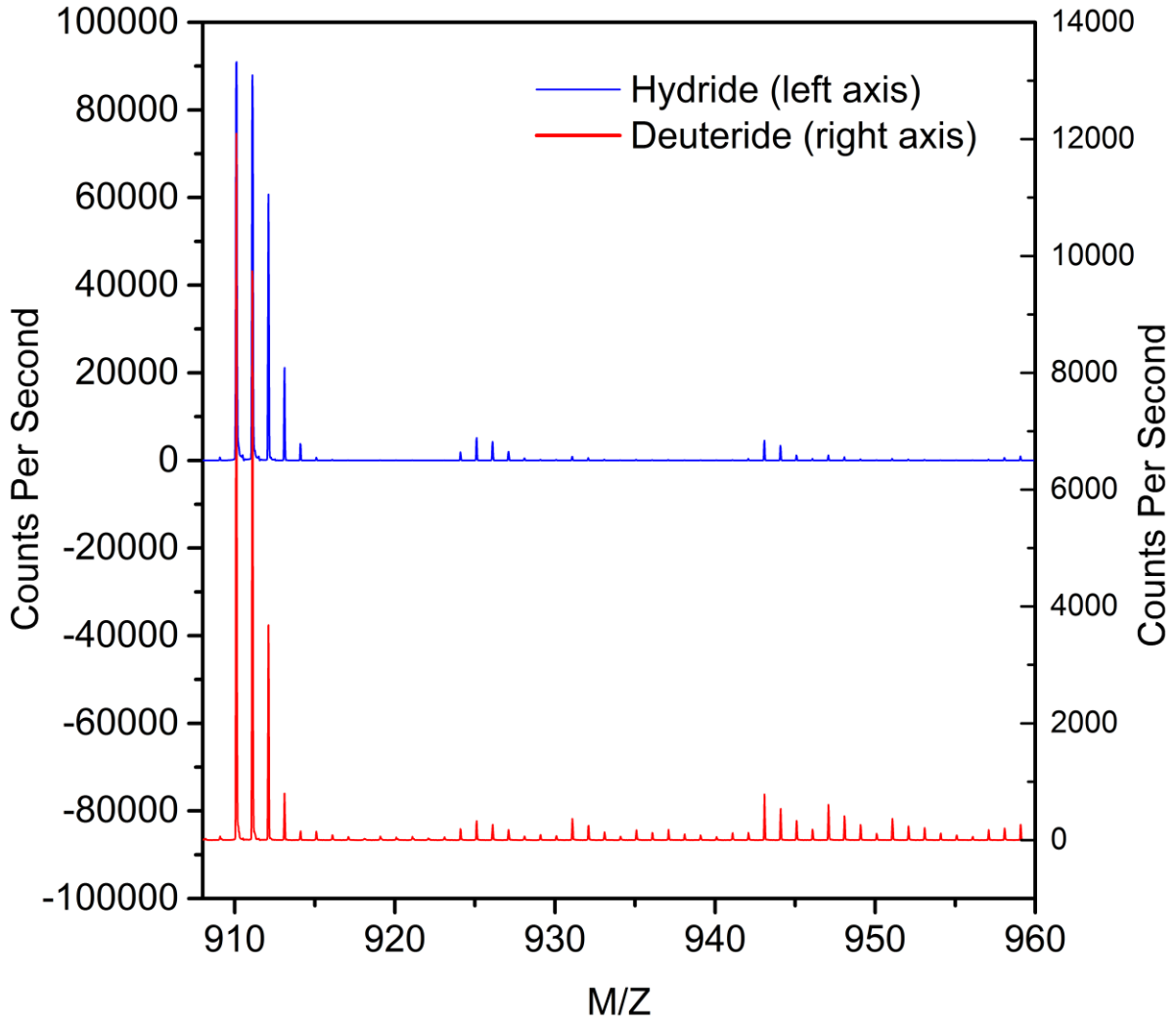

Figure S8: MALDI-TOF-MS spectra for the concentrated soluble matter of the remaining filtrate from the reaction between N-DMBI or d-N-DMBI and $PC_{61}BM$.

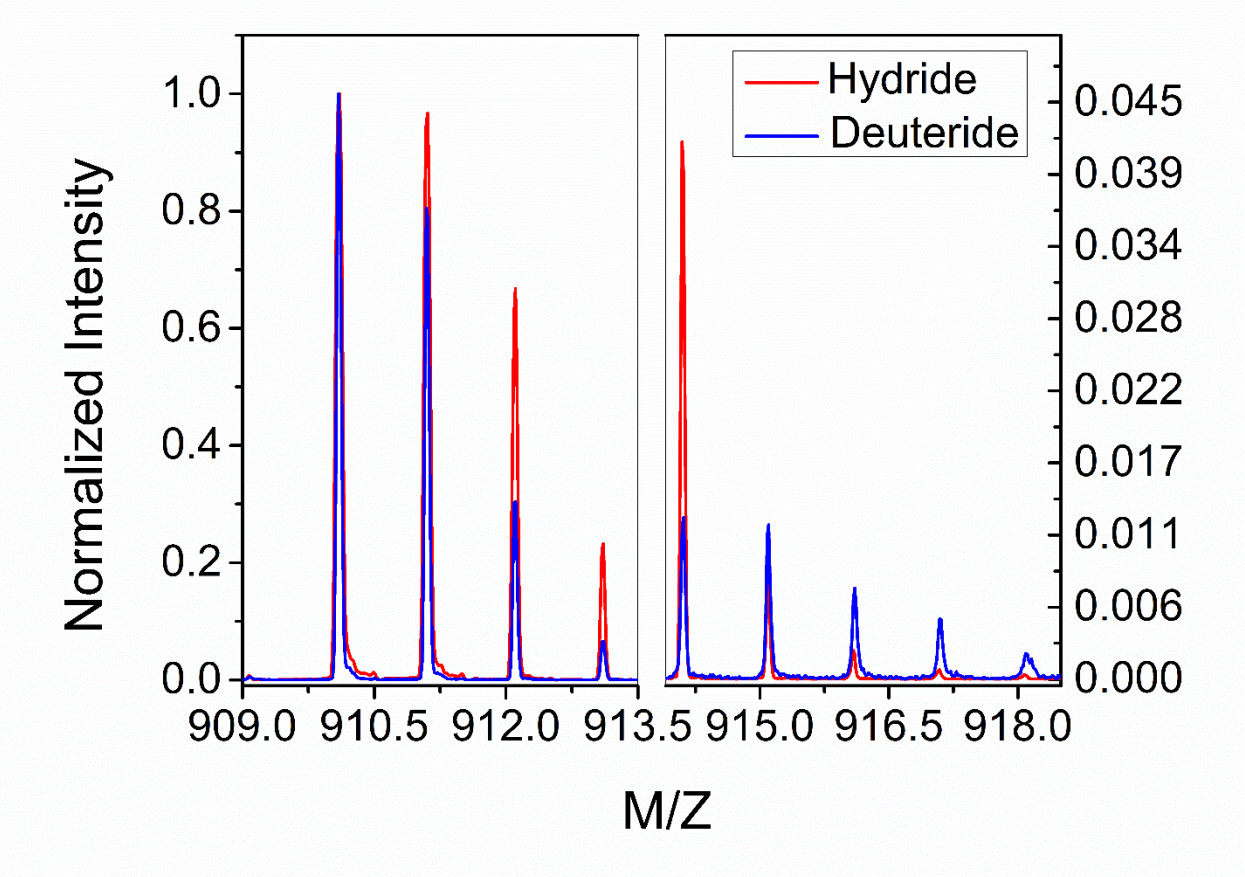

Figure S9: MALDI-TOF-MS spectra expanded around the $PC_{61}BM$ mass for the concentrated soluble matter of the remaining filtrate from the reaction between N-DMBI or d-N-DMBI and $PC_{61}BM$.

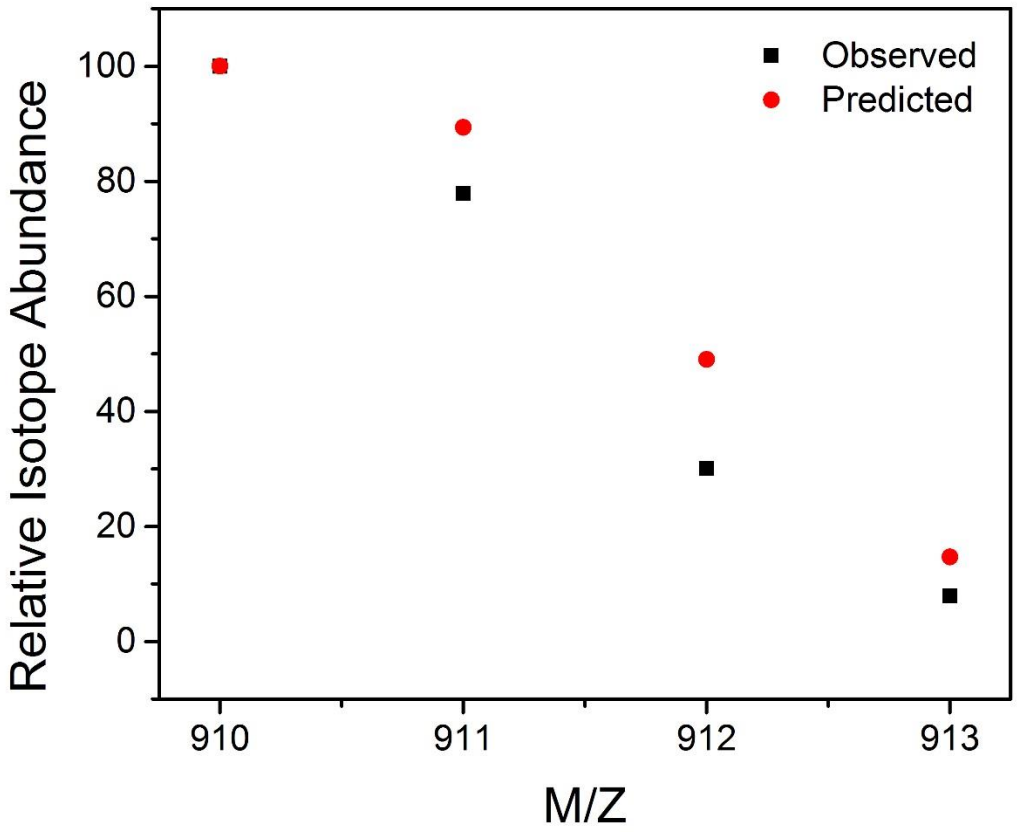

Figure S10: Comparison of predicted and observed relative isotope abundance for concentrated filtrate left from the reaction between N-DMBI and $PC_{61}BM$. The higher isotope masses are present in a greater abundance than for $PC_{61}BM$ consistent with some degree of hydrogenation.

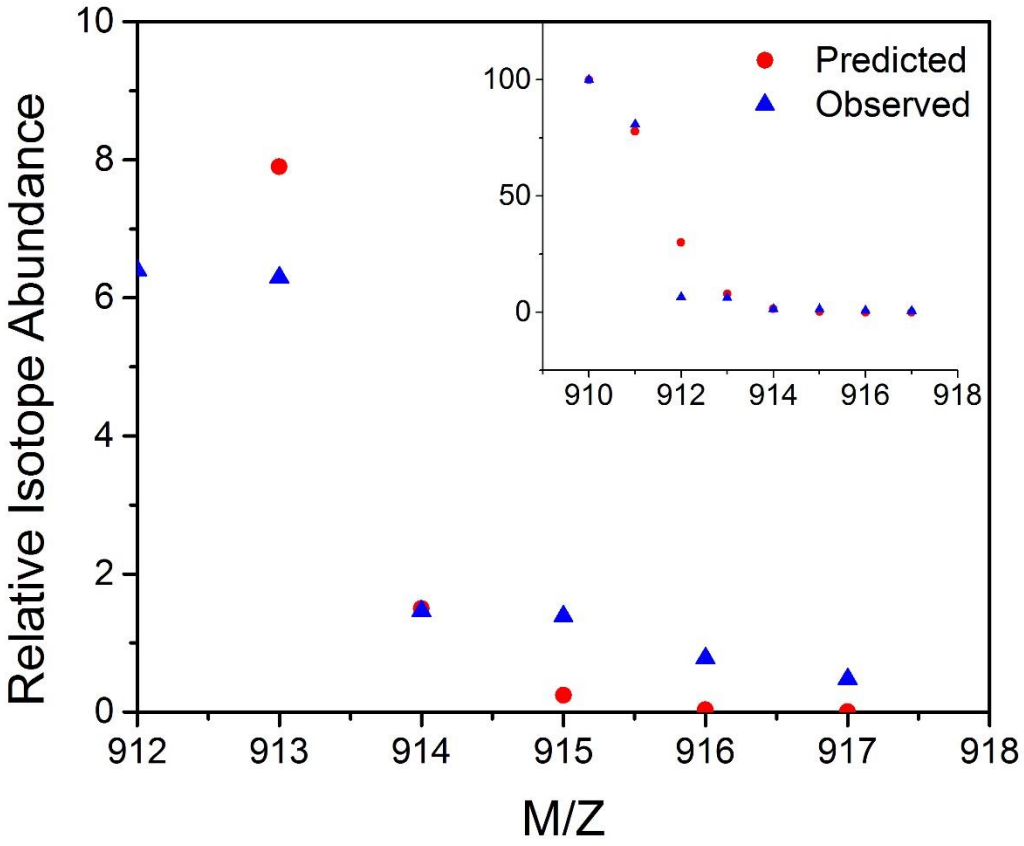

Figure S11: Comparison of predicted and observed relative isotope abundance for concentrated filtrate left from the reaction between d-N-DMBI and $PC_{61}BM$. d-N-DMBI gave an enhancement of even higher isotope masses than N-DMBI, but the effect was minimal on the lower mass peaks (inset).

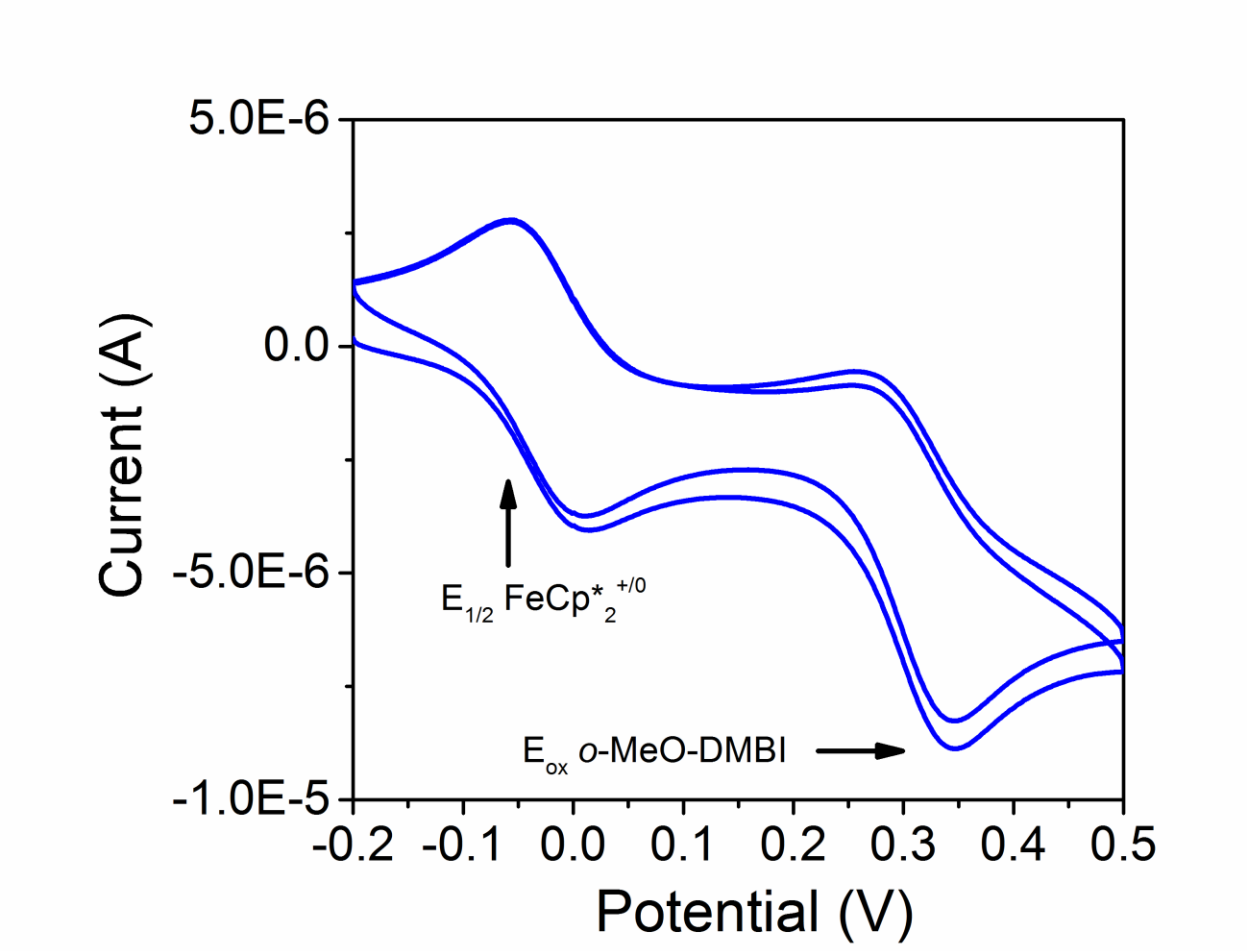

Figure S12: CV data for the oxidation of *o*-MeO-DMBI with the internal reference $FeCp^*_2{}^{+/0}$ shown. The actual value is given in Table S2.

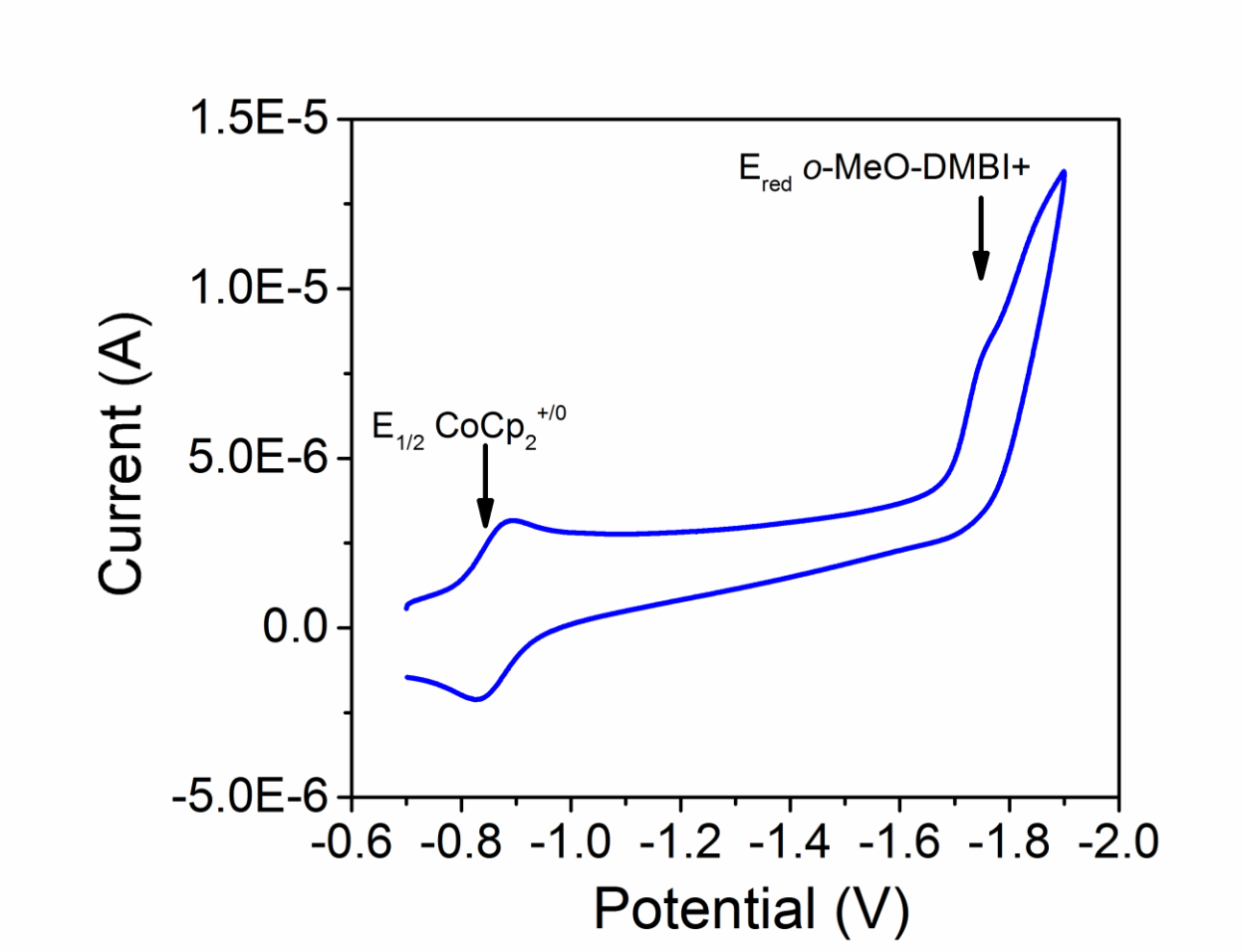

Figure S13: CV data for the reduction of *o*-MeO-DMBI+ with the internal reference $CoCp_2$ shown. The actual value is given in Table S2.

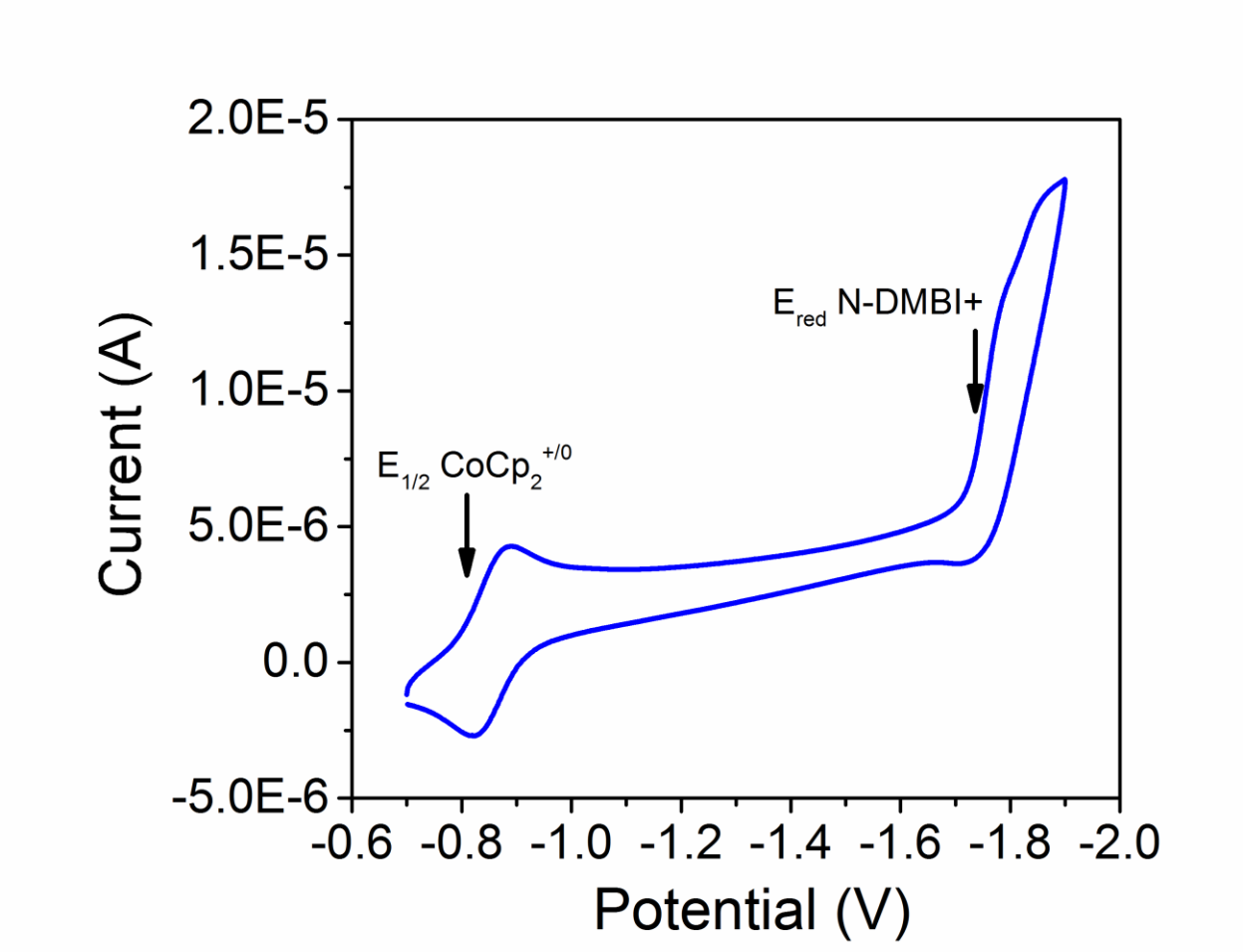

Figure S14: CV data for the reduction of N-DMBI+ with the internal reference $CoCp_2$ shown. The actual value is given in Table S2.

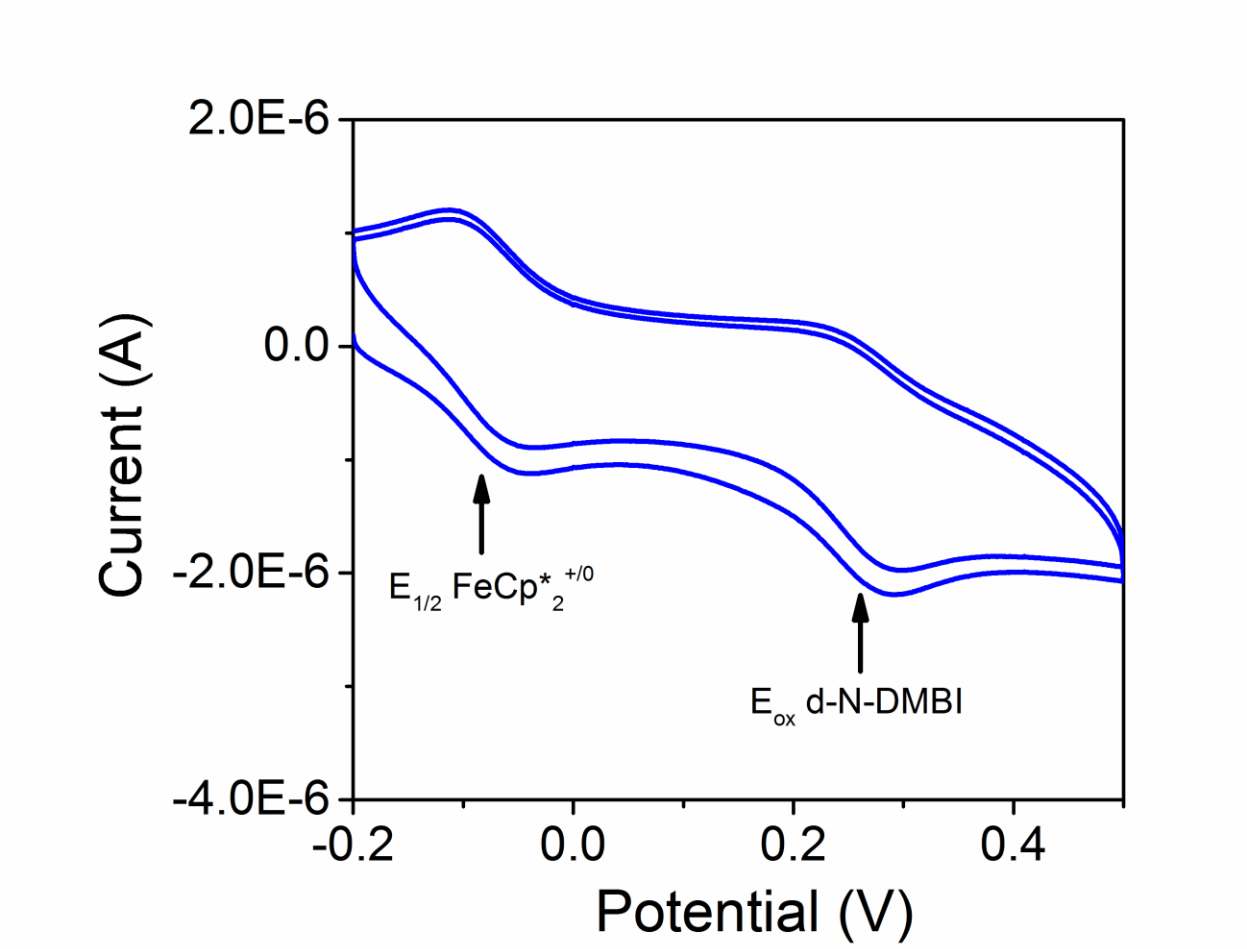

Figure S15: CV data for the oxidation of d-N-DMBI with the internal reference $FeCp^*_2{}^{+/0}$ shown. The actual value is given in Table S2.

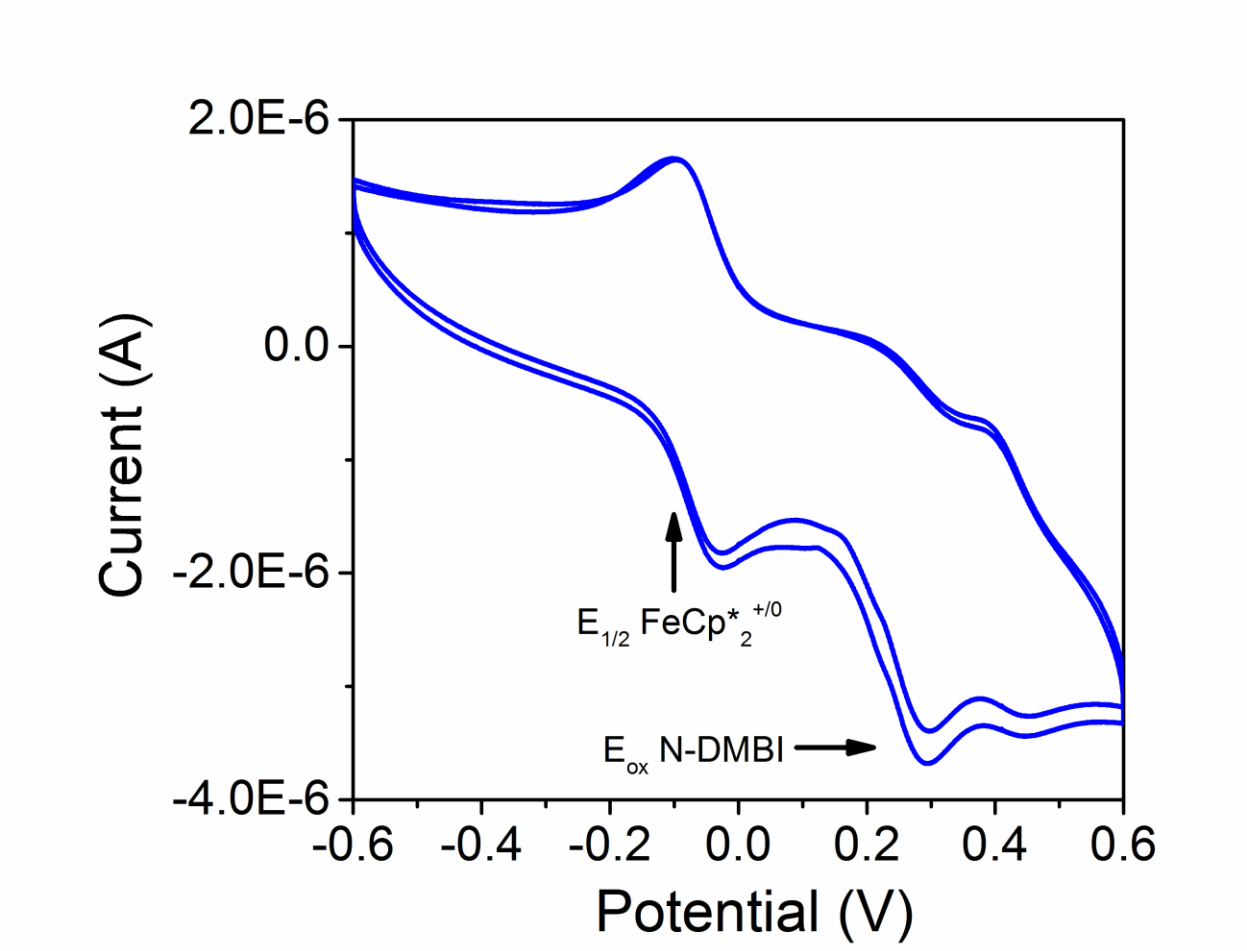

Figure S16: CV data for the oxidation of N-DMBI with the internal reference $FeCp^*_2{}^{+/0}$ shown. The actual value is given in Table S2.

Dopant	Solvent	E_a (kJ·mol^{-1})	$\Delta H^{\neq}$ (kJ·mol^{-1})	$\Delta S^{\neq}$ (J·mol^{-1}·K^{-1})	$\Delta G^{\neq}$ (300 K) (kJ·mol^{-1})
N-DMBI	ClBz	60.5	57.8	-92.0	85.4
		0.63 eV	0.60 eV		0.88 eV
N-DMBI	1:1 Benzonitrile:ClBz	59.7	57.0	-90.3	84.0
		0.62 eV	0.59 eV		0.87 eV
N-DMBI	Toluene	60.4	57.5	-91.1	84.9
		0.63 eV	0.60 eV		0.88 eV
d-N-DMBI	ClBz	71.3	68.6	-72.8	90.4
		0.74 eV	0.71 eV		0.94 eV

Table S1: Extracted activation parameters for the doping reaction at 300 K for N-DMBI and d-N-DMBI with $PC_{61}BM$ in the indicated solvent. E_a was extracted from the slope of the ln(k) vs. 1/T plot using the linear form of the Arrhenius equation ($\ln(k) = -E_a/RT + \ln(A)$). $\Delta H^{\neq}$, $\Delta S^{\neq}$, and $\Delta G^{\neq}$ were extracted from the plot of ln(k/T) vs 1/T using the linear form of the Eyring equation ($\ln(k/T) = -\Delta H^{\neq}/RT + \ln(k_B/h) + (\Delta S^{\neq}/R)$).

Compound	E_{ox} vs. $FeCp_2^{+/0}$ (V)	E_{red} vs. $FeCp_2^{+/0}$ (V)
N-DMBI	-0.14	
d-N-DMBI	-0.13	
$[N\text{-}DMBI]^+$		-2.23
o-MeO-DMBI	-0.13	
$[MeO\text{-}DMBI]^+$		-2.22

Table S2: Electrochemical data for N-DMBI, d-N-DMBI, *o*-MeO-DMBI, and the corresponding imidazolium cations as measured by cyclic voltammetry in 0.1 M $TBAPF_6$/MeCN at 50 mV/s. Notably the values found for N-DMBI reduction and oxidation are comparable to the values found in reference 17. Samples were referenced to $FeCp^*_2^{+/0}$, or $CoCp_2^{+/0}$ which and then corrected to $FeCp_2^{+/0}$.

Ultraviolet and Inverse Photoelectron Spectroscopies (UPS and IPES):

The samples for photoelectron spectroscopy measurements were prepared by spin coating under N_2 atmosphere from solutions containing 5.2 mg/mL 6,13-bis(triisopropylsilylethynyl)pentacene (TIPS-pentacene), 8 mg/mL $PC_{61}BM$, and 20 mg/mL *o*-MeO-DMBI in toluene. Doping was achieved by mixing the matrix and dopant solutions at the desired weight ratios. Tin-doped indium oxide (ITO) was used as the substrate, except in the case of the pure *o*-MeO-DMBI sample, where a better film formation was found on air-exposed gold. For the photoelectron spectroscopy measurements the samples were transferred into an ultra-high vacuum system. Samples containing the n-dopant were transferred via a transport system without air exposure, while the more stable films were exposed to air for a few seconds during the loading process. .

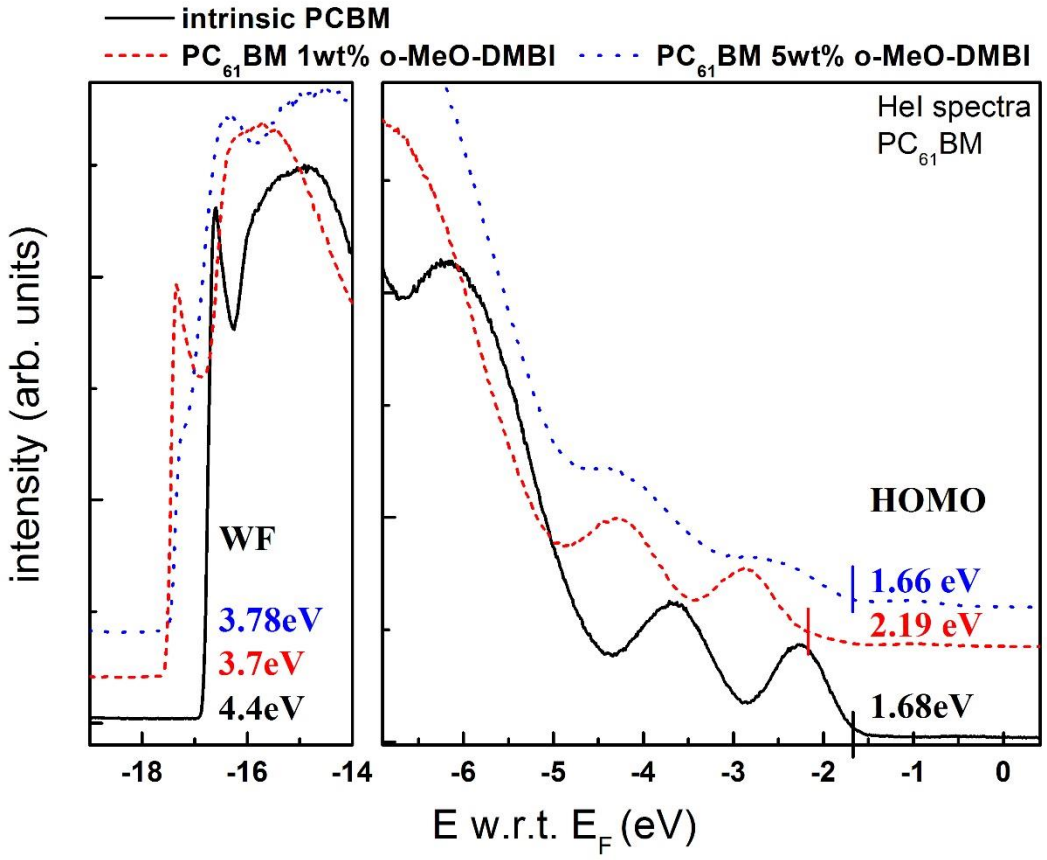

Figure S17: UPS spectra for $PC_{61}BM$ and *o*-MeO-DMBI doped $PC_{61}BM$ on ITO. The strong shift between the intrinsic and 1 wt% doped sample indicates the efficient doping effect of *o*-MeO-DMBI in this matrix. In the case of the 5 wt% doping the features get significantly broadened by the presence of the dopants.

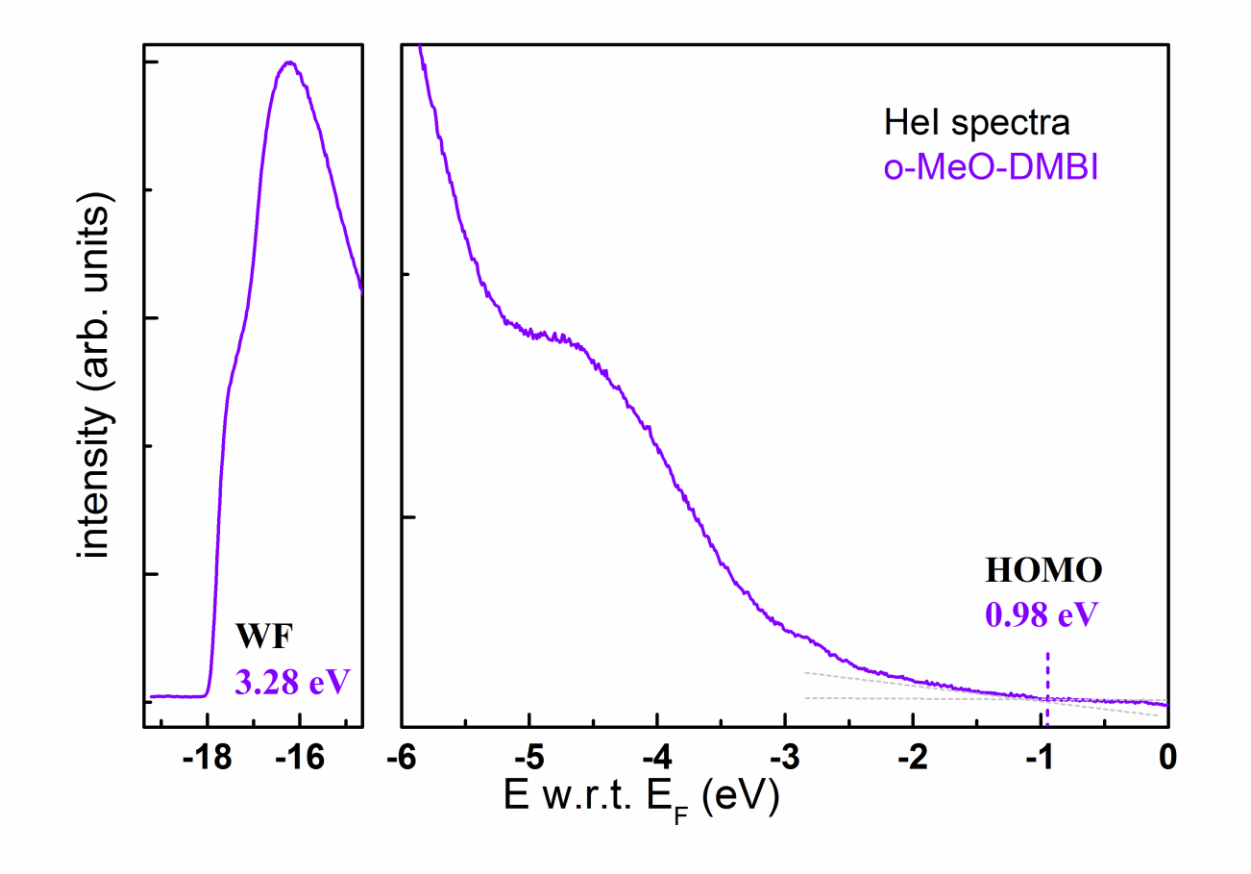

Figure S18: UPS spectra for pure *o*-MeO-DMBI on air-exposed gold.

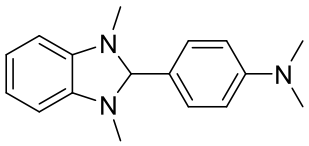

Top: ^{1}H-NMR (D_6-DMSO)

Bottom: ^{13}C-NMR (D_6-DMSO)

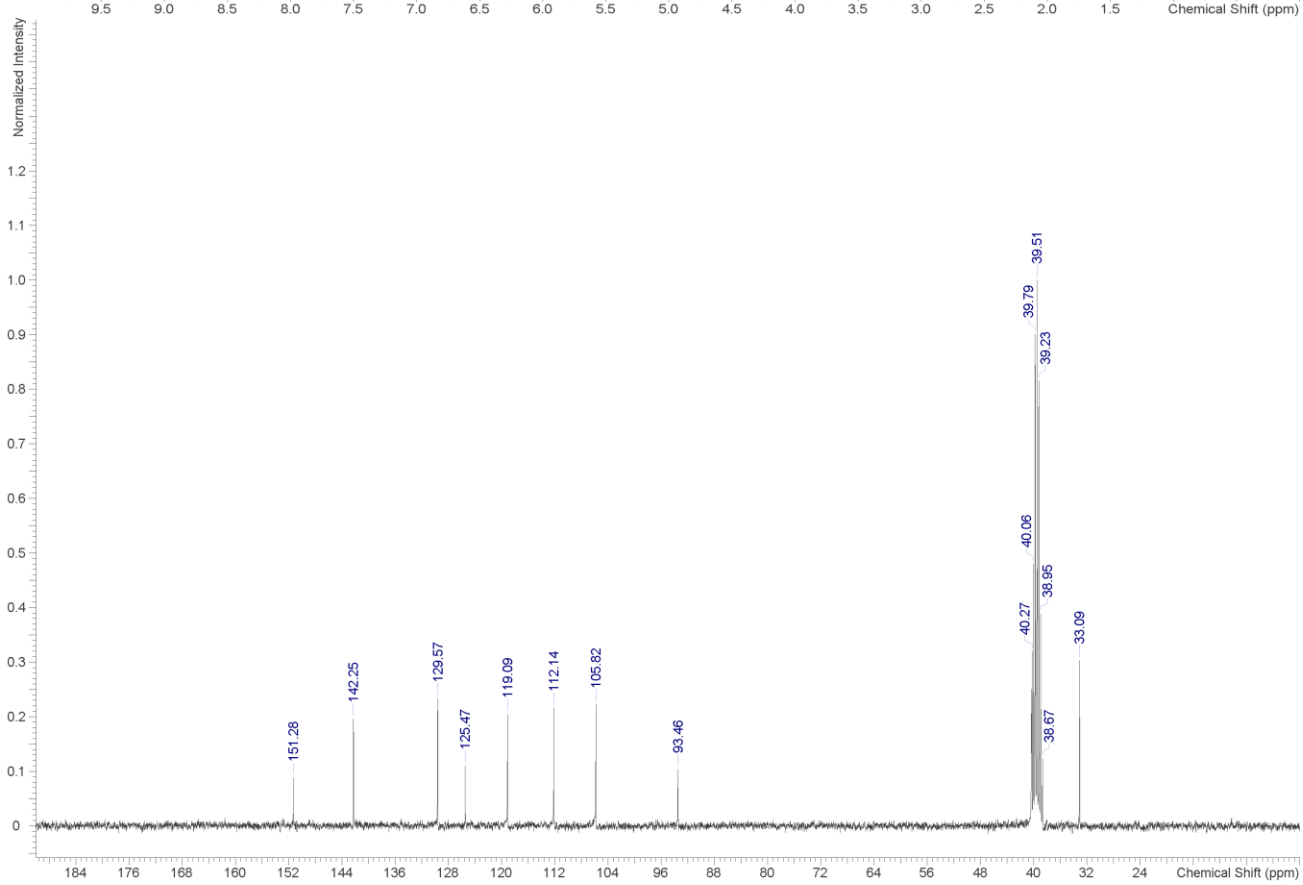

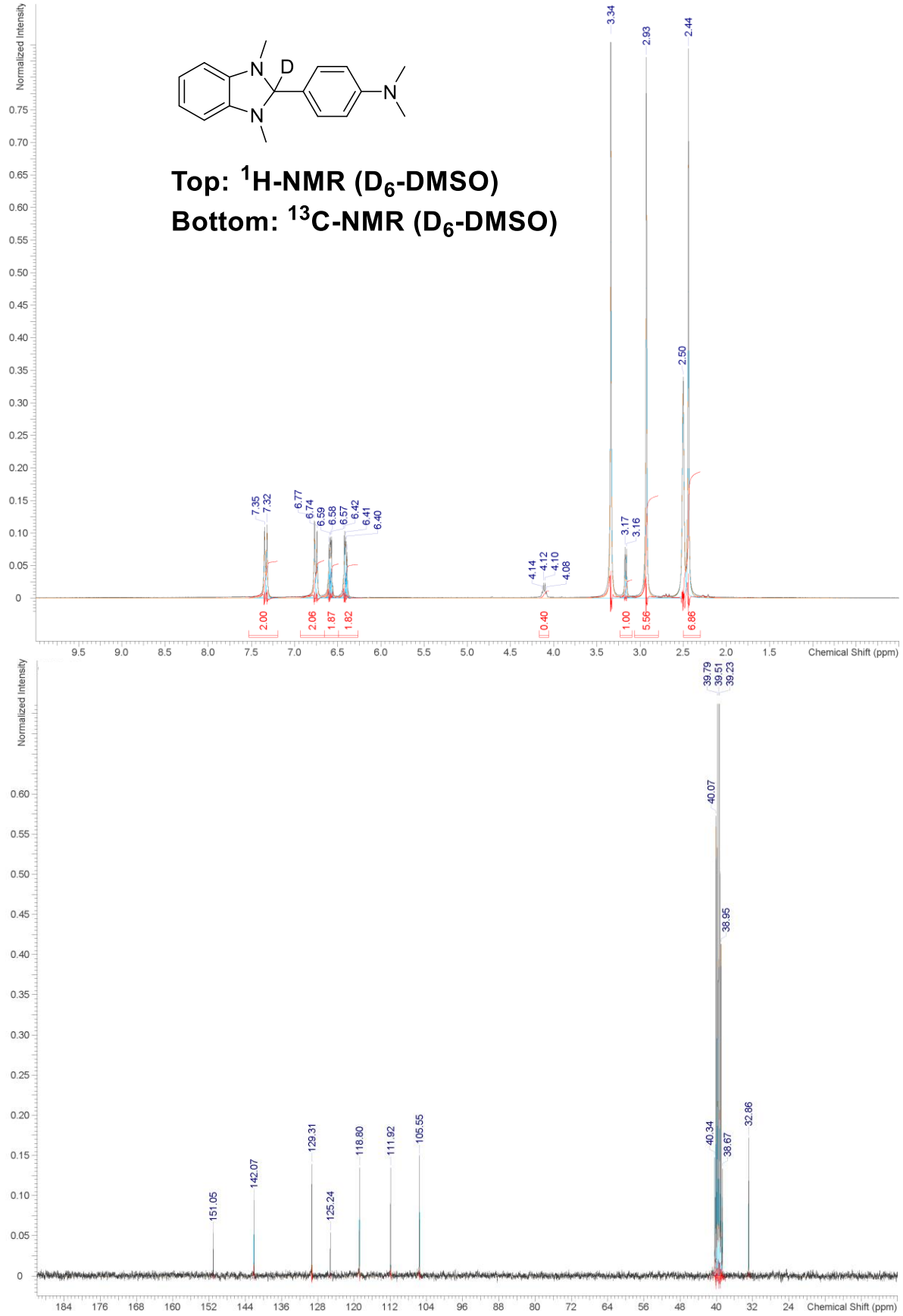
Top: ^{1}H-NMR (D_6-DMSO)
Bottom: ^{13}C-NMR (D_6-DMSO)
Normalized Intensity
Chemical Shift (ppm)
7.35
7.32
6.77
6.74
6.59
6.58
6.57
6.42
6.41
6.40
4.14
4.12
4.10
4.08
3.34
3.17
3.16
2.93
2.50
2.44
2.00
2.06
1.87
1.82
0.40
1.00
5.56
6.86
39.79
39.51
39.23
40.07
38.95
40.34
38.67
32.86
151.05
142.07
129.31
125.24
118.80
111.92
105.55

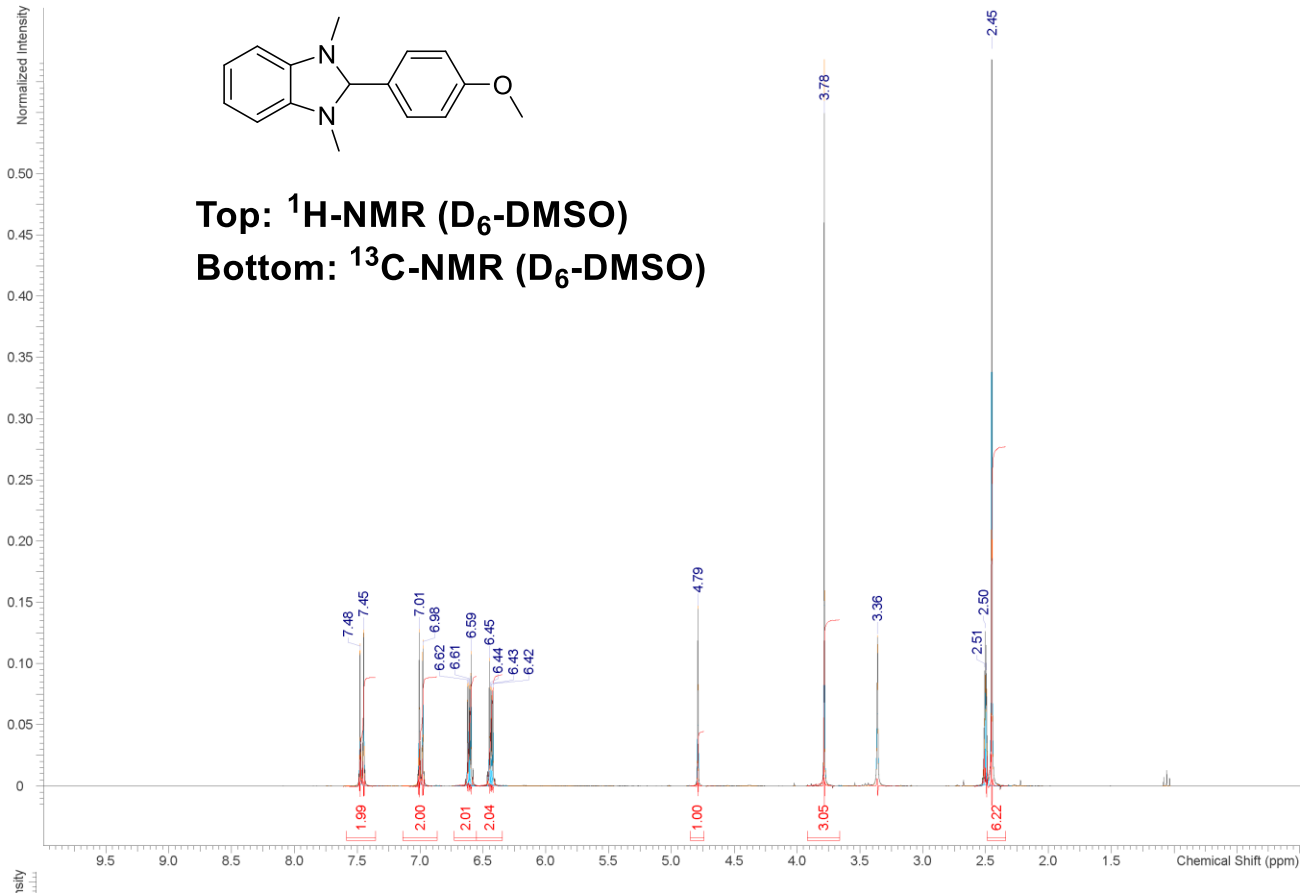

Top: ^{1}H-NMR (D_6-DMSO)

Bottom: ^{13}C-NMR (D_6-DMSO)

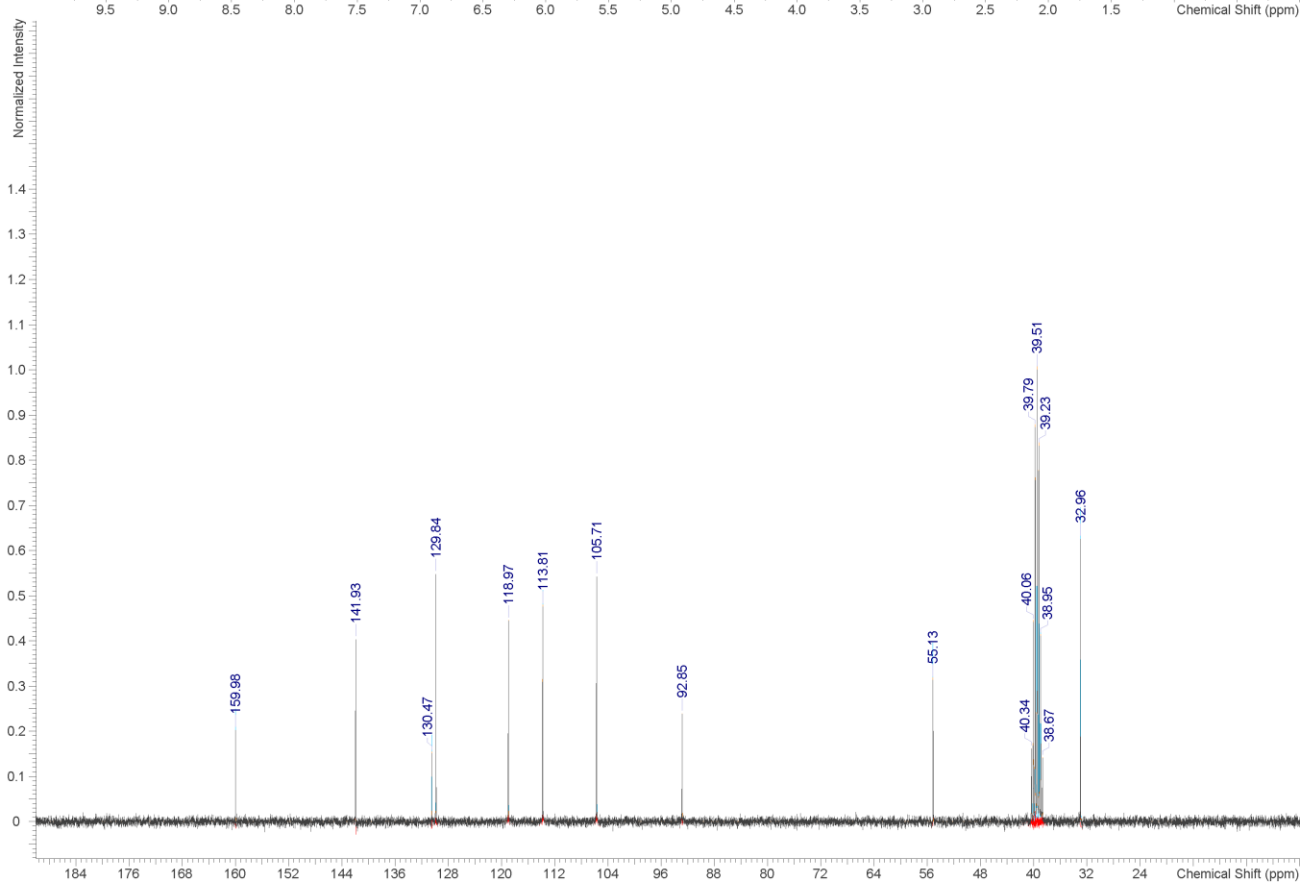

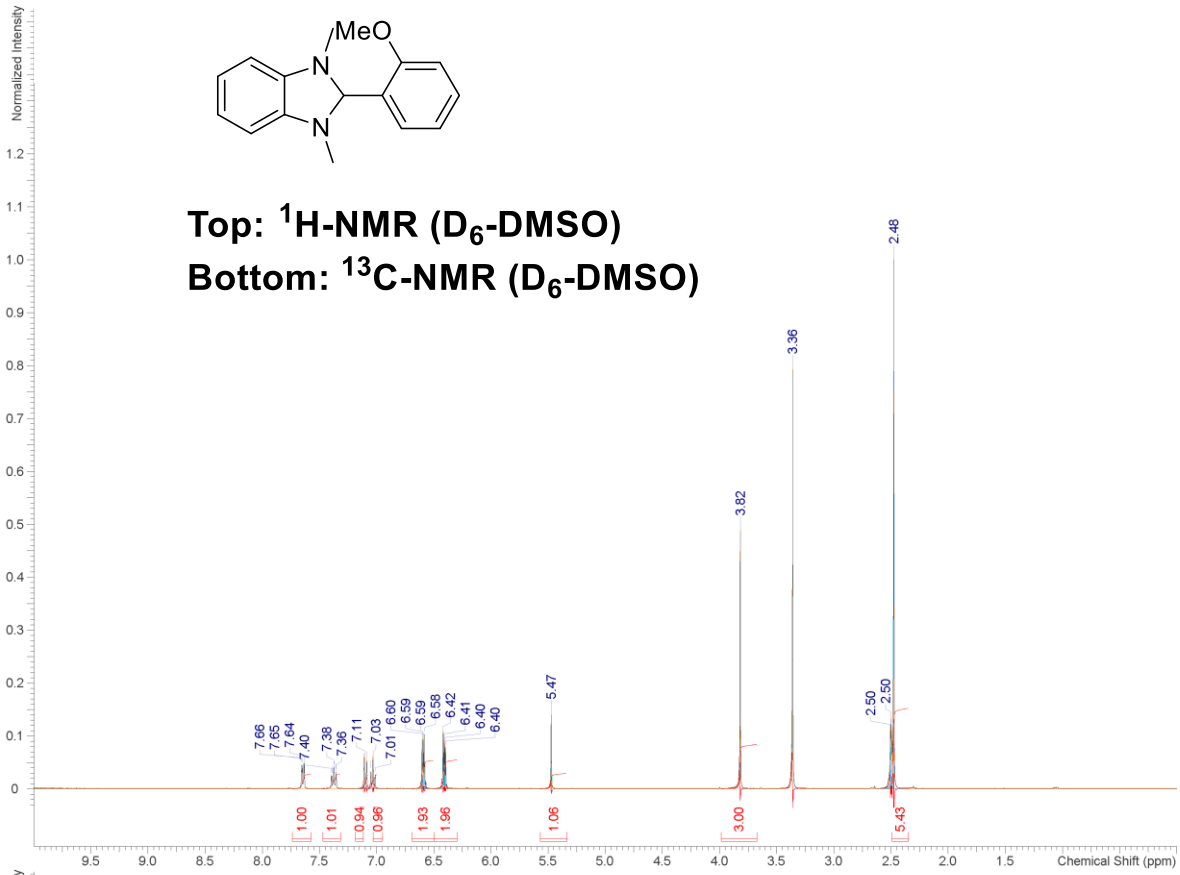
MeO
N
N
Top: ^{1}H-NMR (D_6-DMSO)
Bottom: ^{13}C-NMR (D_6-DMSO)
Normalized Intensity
7.66
7.65
7.64
7.40
7.38
7.36
7.11
7.03
7.01
6.60
6.59
6.59
6.58
6.42
6.41
6.40
6.40
5.47
3.82
3.36
2.50
2.50
2.48
1.00
1.01
0.94
0.96
1.93
1.96
1.06
3.00
5.43
Chemical Shift (ppm)

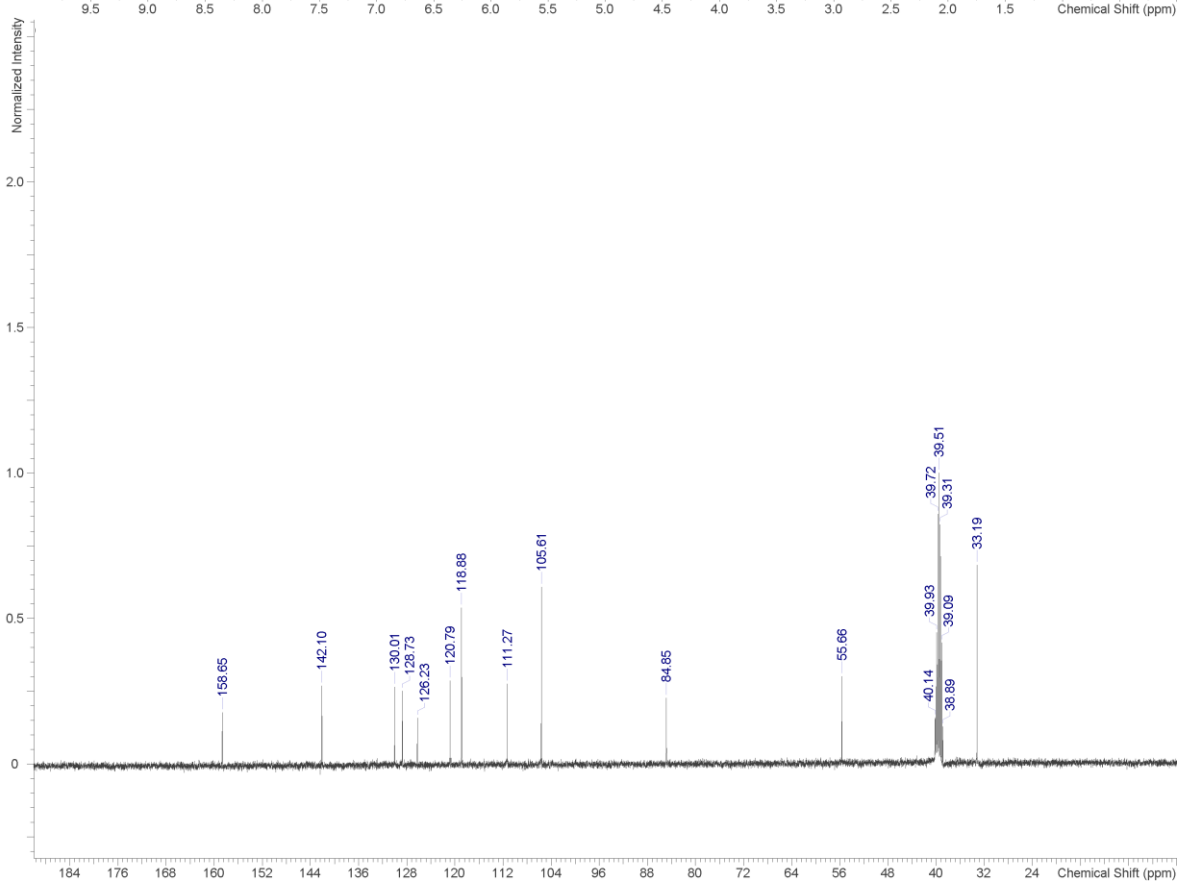
Normalized Intensity
158.65
142.10
130.01
128.73
126.23
120.79
118.88
111.27
105.61
84.85
55.66
39.93
39.72
39.51
39.31
39.09
38.89
40.14
33.19
Chemical Shift (ppm)

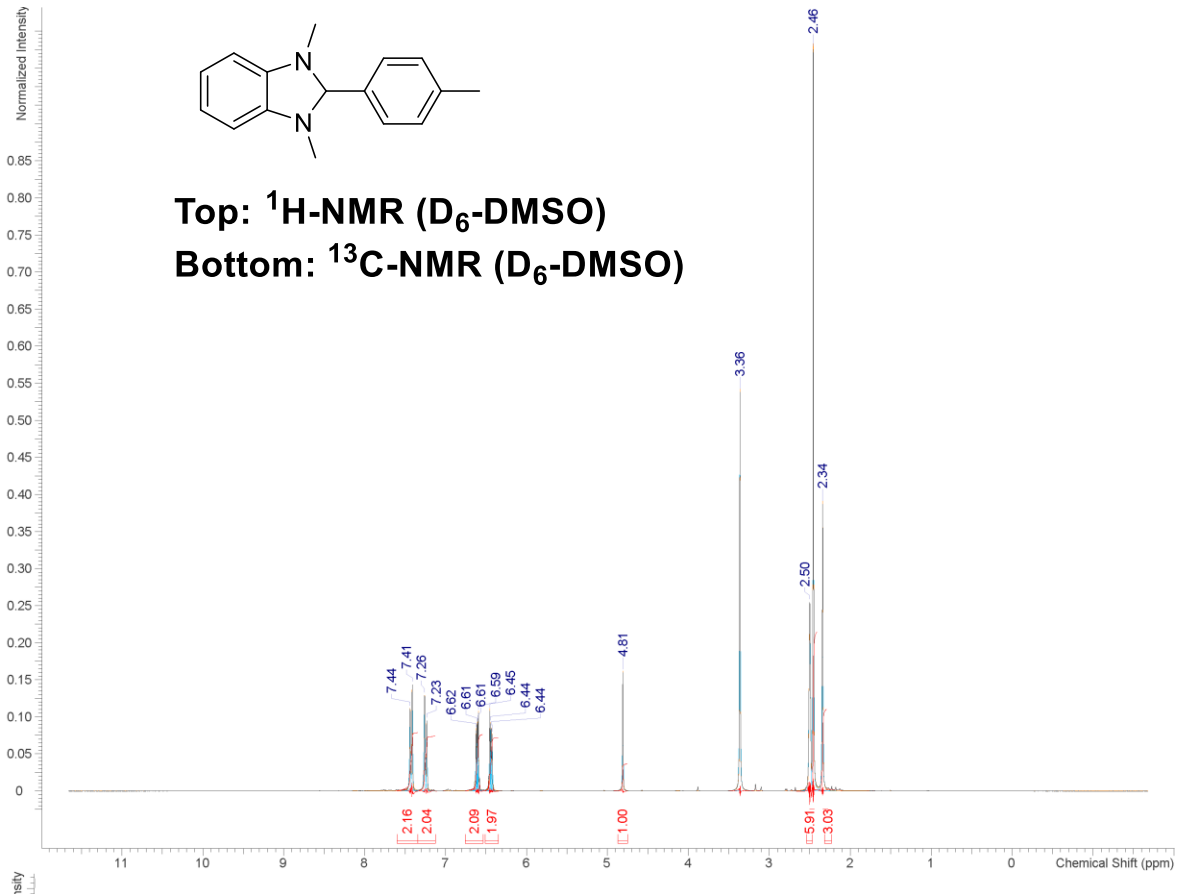

Top: ^{1}H-NMR (D_6-DMSO)

Bottom: ^{13}C-NMR (D_6-DMSO)

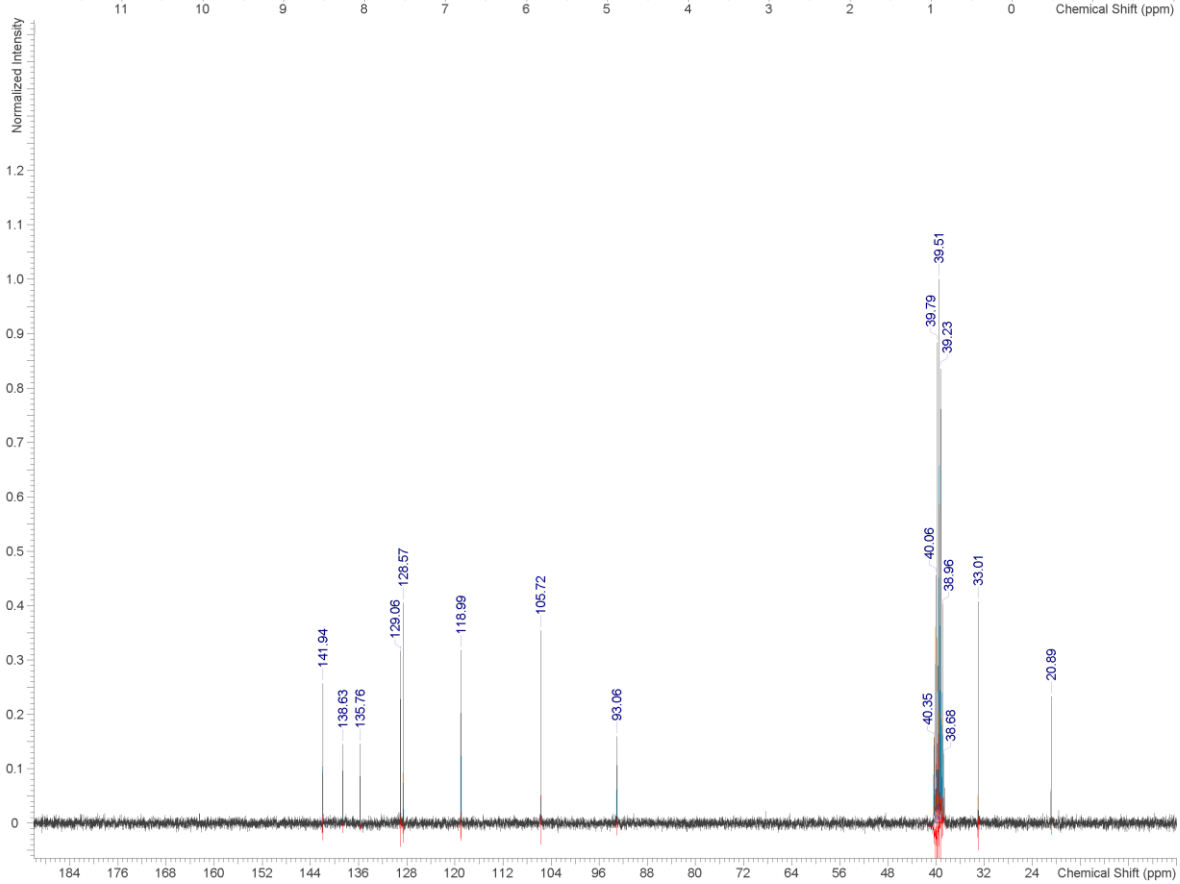

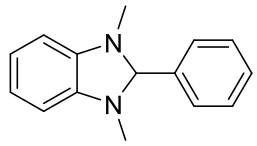

Top: ^{1}H-NMR (D_6-DMSO)

Bottom: ^{13}C-NMR (D_6-DMSO)

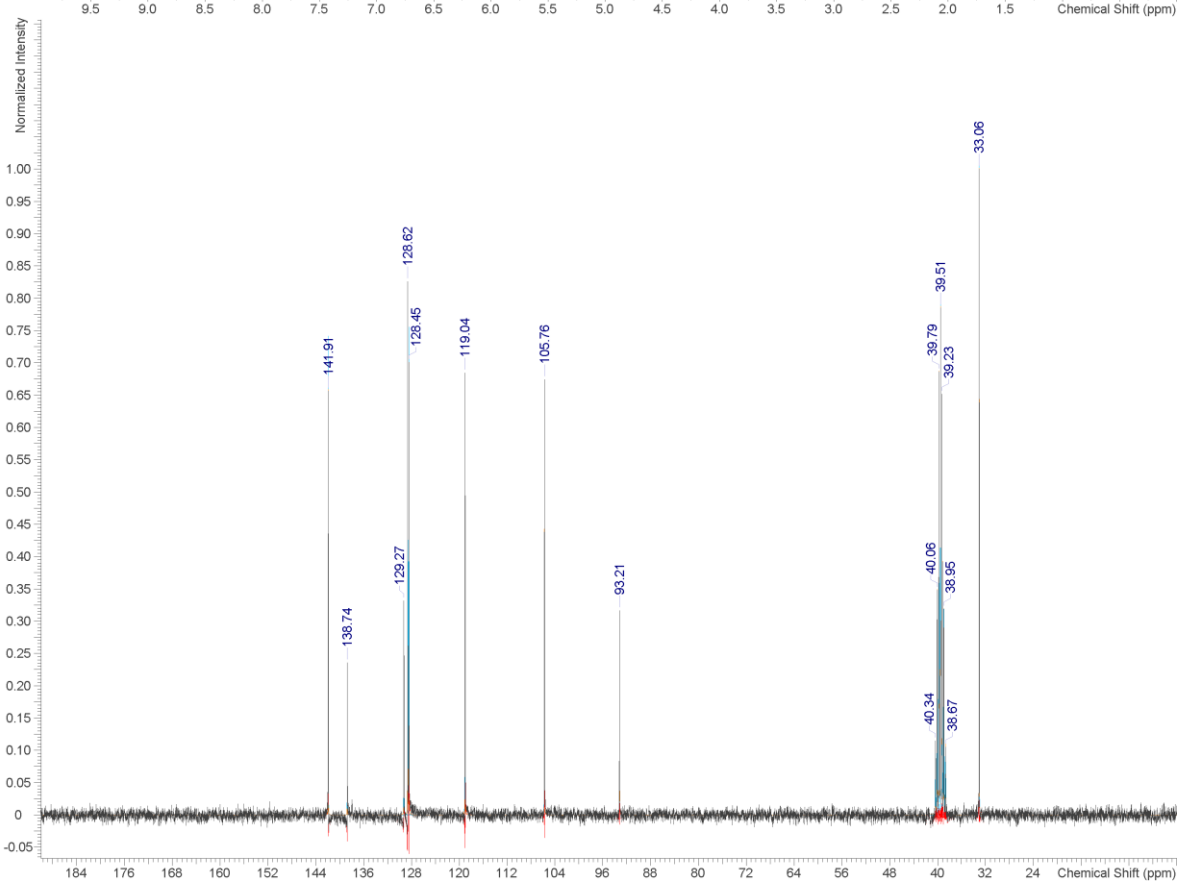

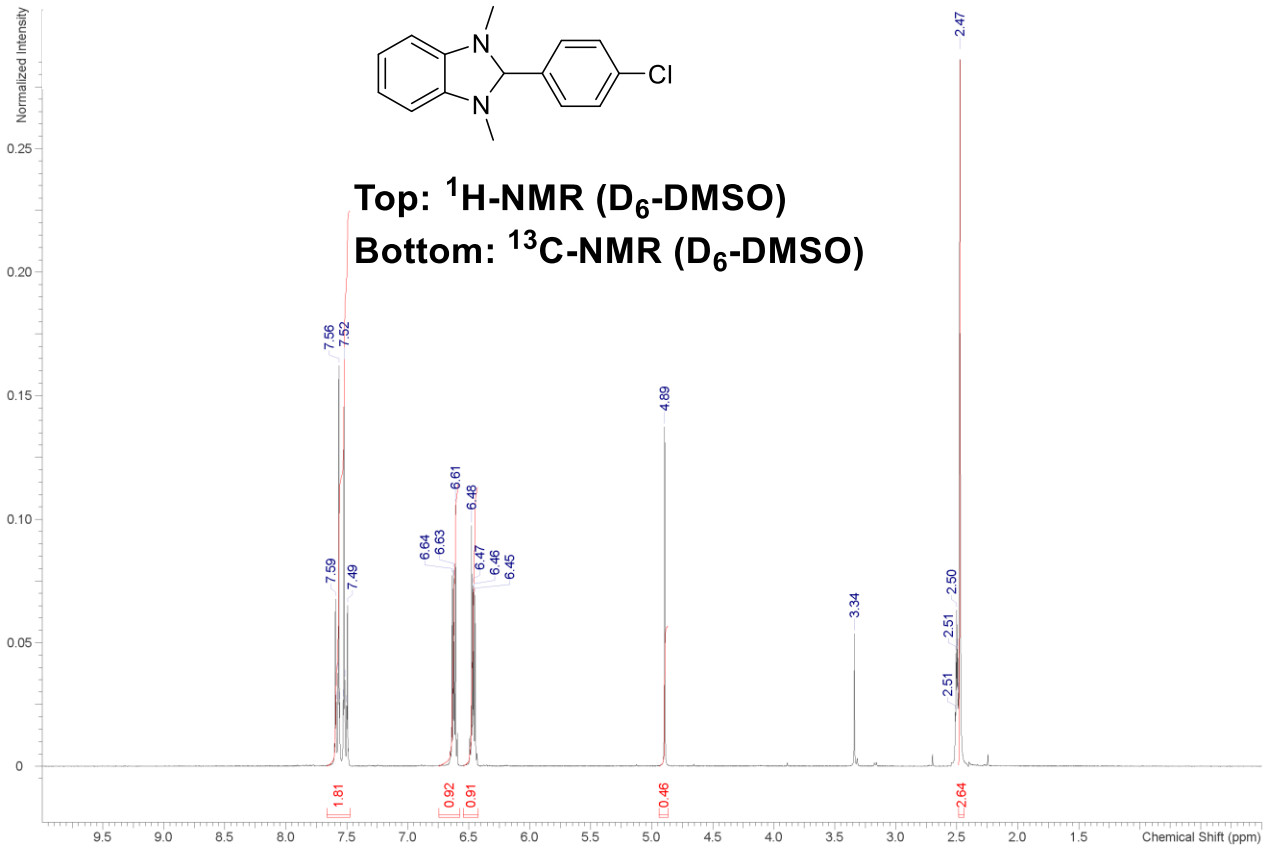
Cl
N
N
Top: ^{1}H-NMR (D_6-DMSO)
Bottom: ^{13}C-NMR (D_6-DMSO)
Normalized Intensity
Chemical Shift (ppm)
7.56
7.52
7.59
7.49
6.64
6.63
6.61
6.48
6.47
6.46
6.45
4.89
3.34
2.50
2.51
2.51
2.47
1.81
0.92
0.91
0.46
2.64

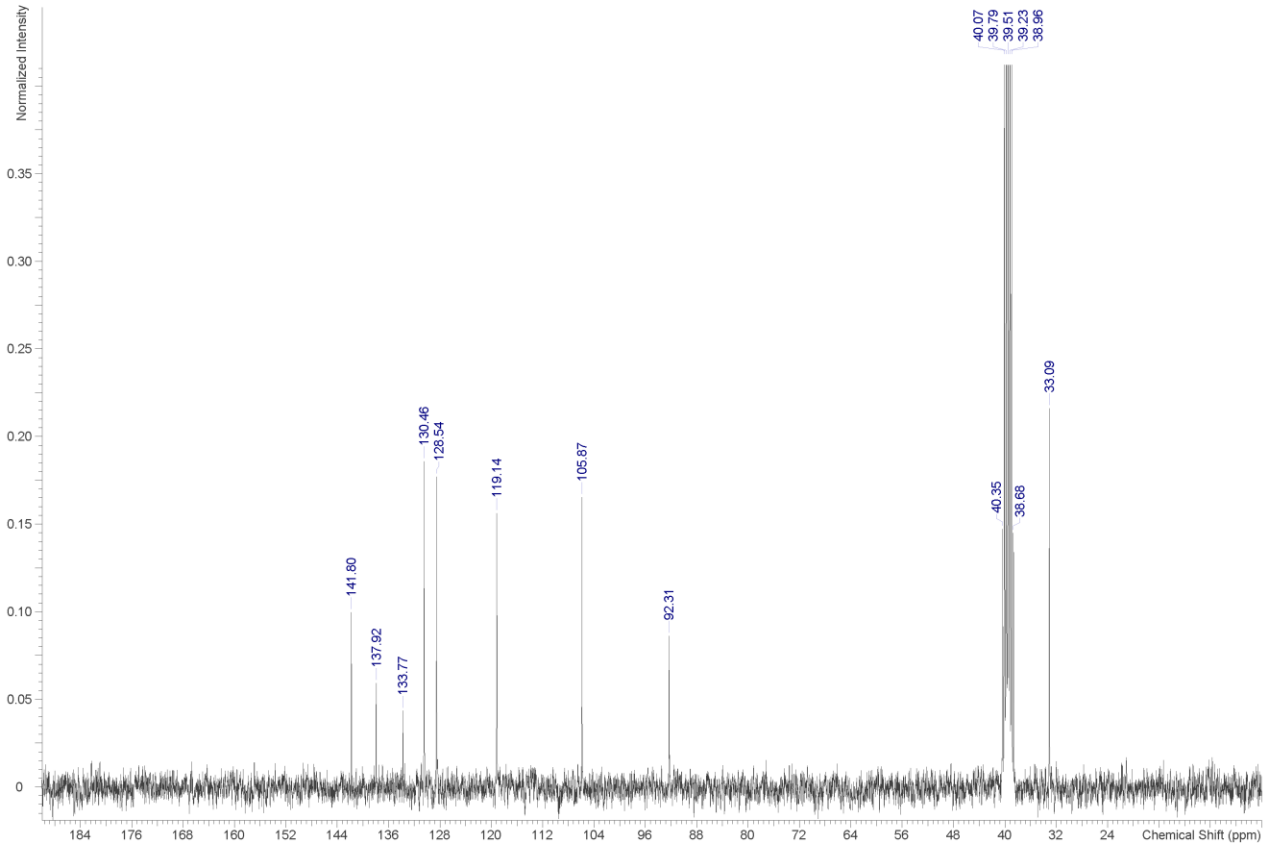
Normalized Intensity
Chemical Shift (ppm)
40.07
39.79
39.51
39.23
38.96
33.09
40.35
38.68
130.46
128.54
119.14
105.87
141.80
137.92
133.77
92.31

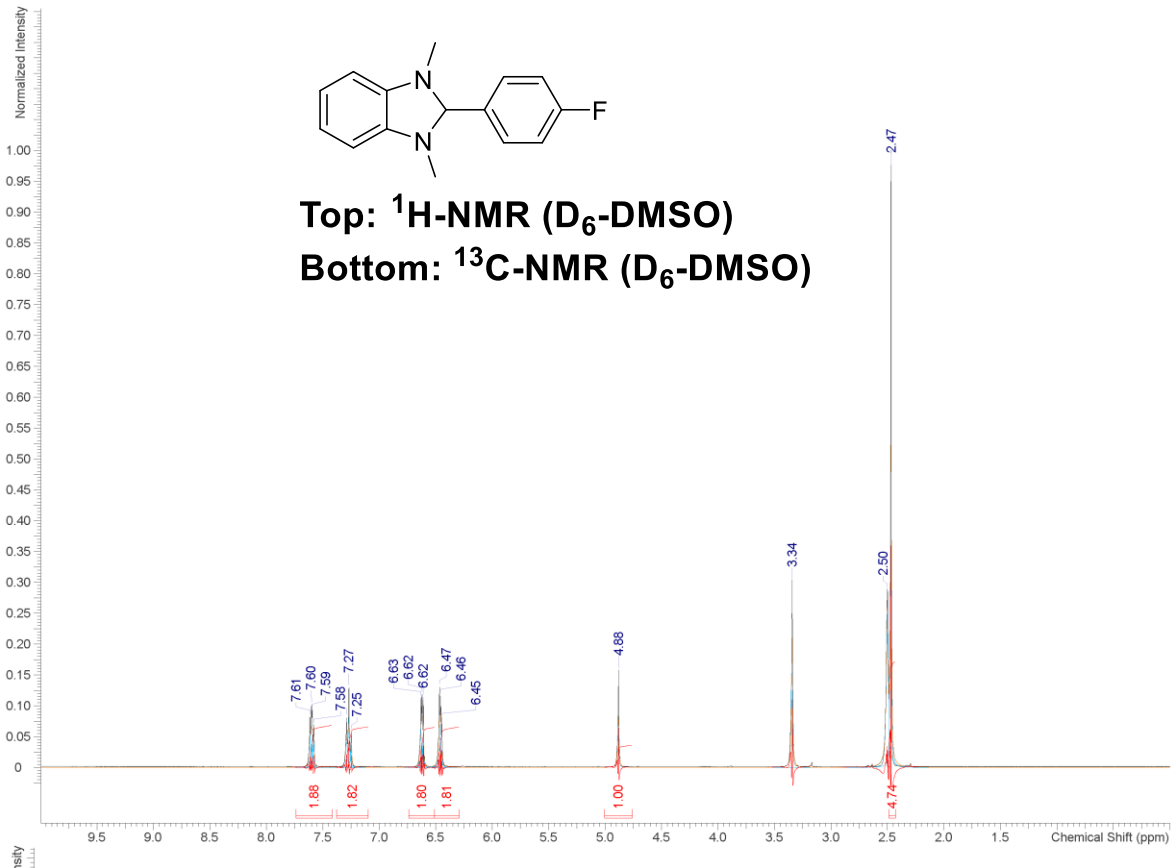
Top: ^{1}H-NMR (D_6-DMSO)
Bottom: ^{13}C-NMR (D_6-DMSO)
Normalized Intensity
Chemical Shift (ppm)
7.61
7.60
7.59
7.58
7.27
7.25
6.63
6.62
6.62
6.47
6.46
6.45
4.88
3.34
2.50
2.47
1.88
1.82
1.80
1.81
1.00
4.74

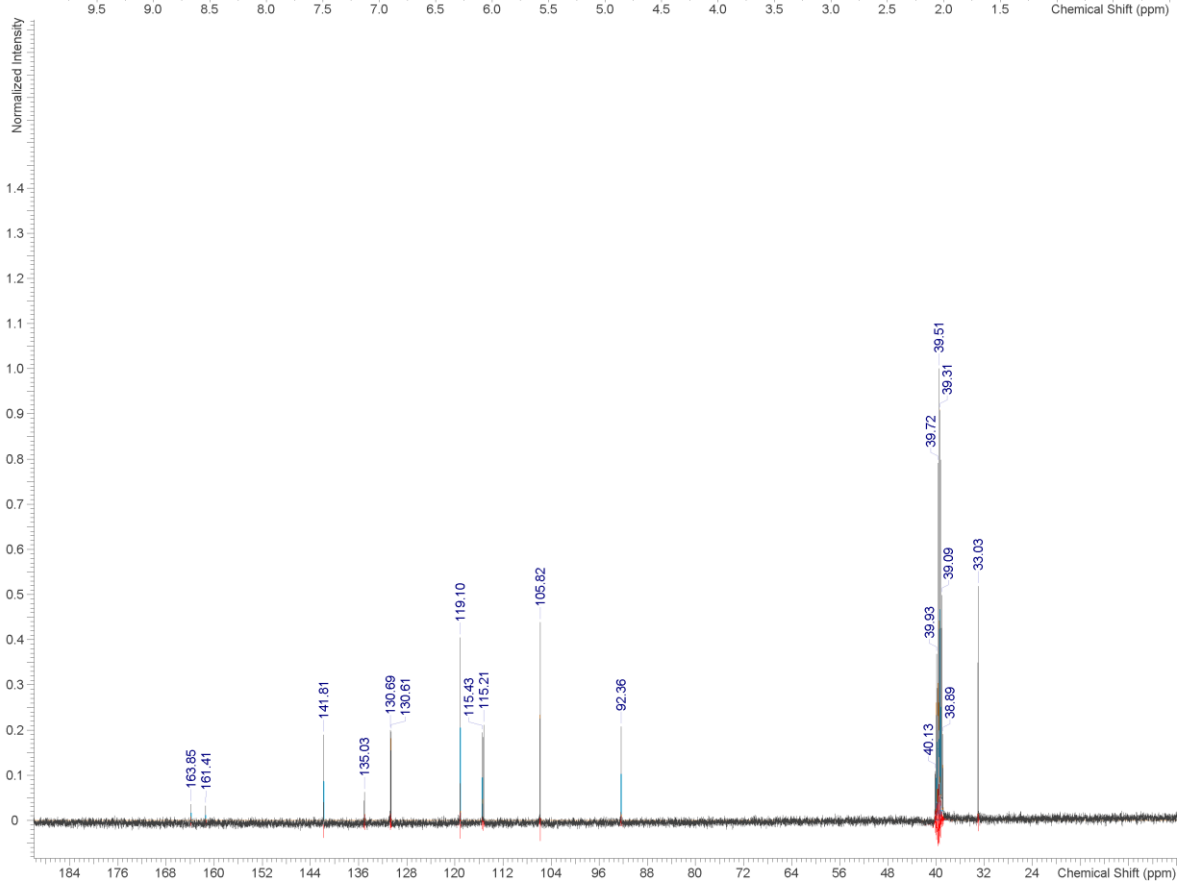
Normalized Intensity
Chemical Shift (ppm)
163.85
161.41
141.81
135.03
130.69
130.61
119.10
115.43
115.21
105.82
92.36
39.93
40.13
39.72
39.51
39.31
39.09
38.89
33.03

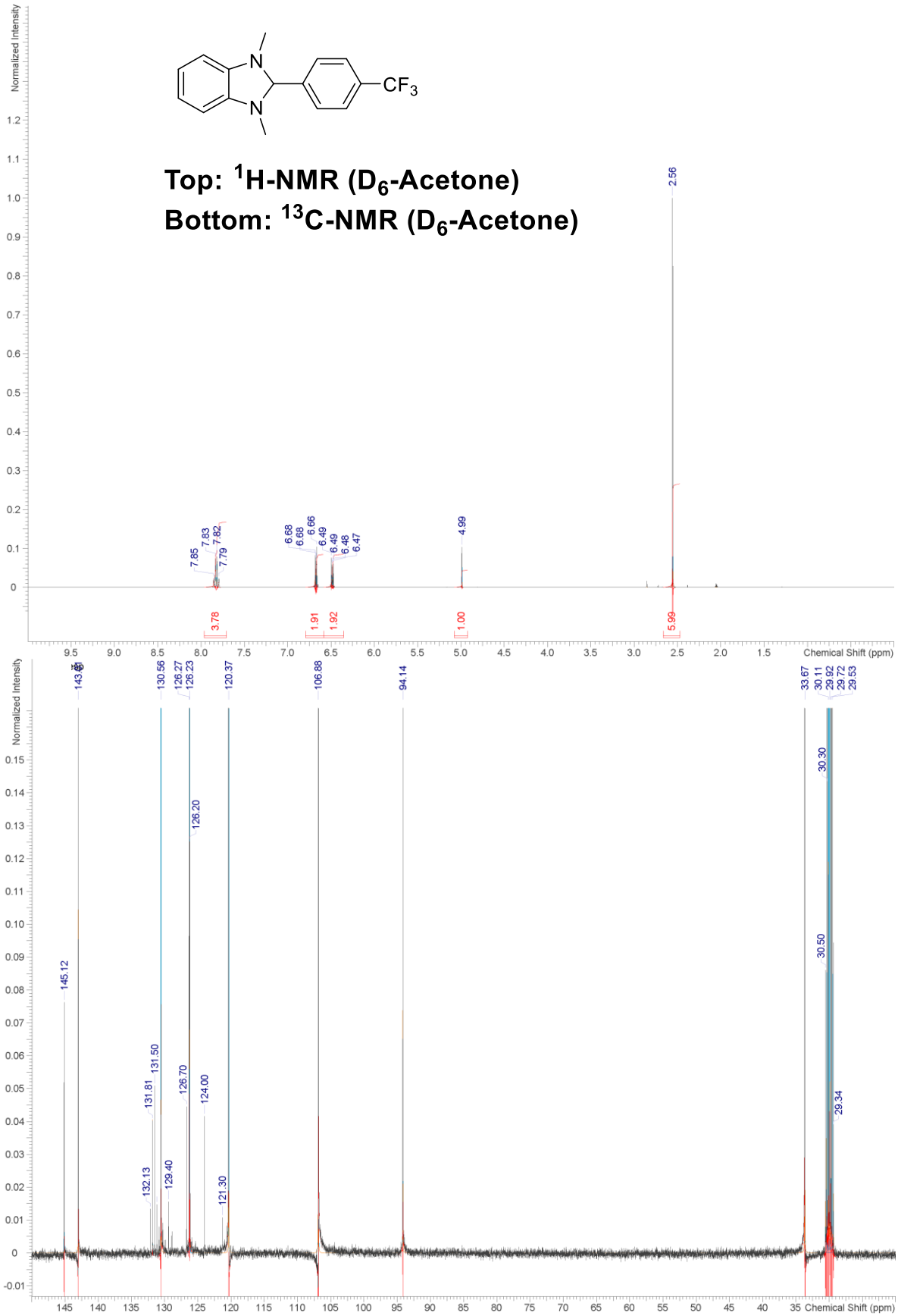
Top: ^{1}H-NMR (D_6-Acetone)
Bottom: ^{13}C-NMR (D_6-Acetone)
Normalized Intensity
Chemical Shift (ppm)
2.56
4.99
7.85
7.83
7.82
7.79
6.68
6.68
6.66
6.49
6.49
6.48
6.47
3.78
1.91
1.92
1.00
5.99
145.12
130.56
126.27
126.23
120.37
106.88
94.14
33.67
30.11
29.92
29.72
29.53
30.30
30.50
29.34
126.20
131.50
131.81
126.70
124.00
132.13
129.40
121.30

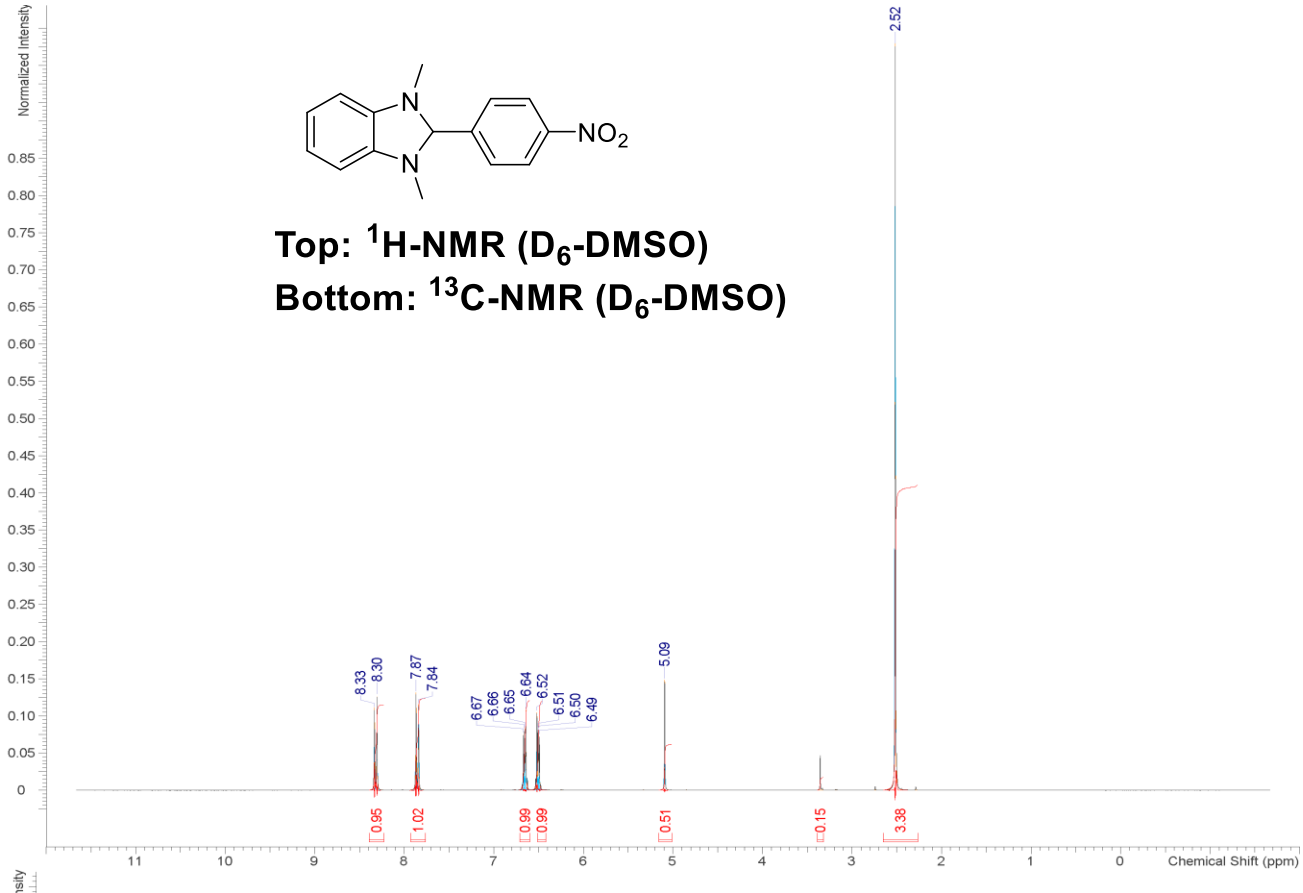

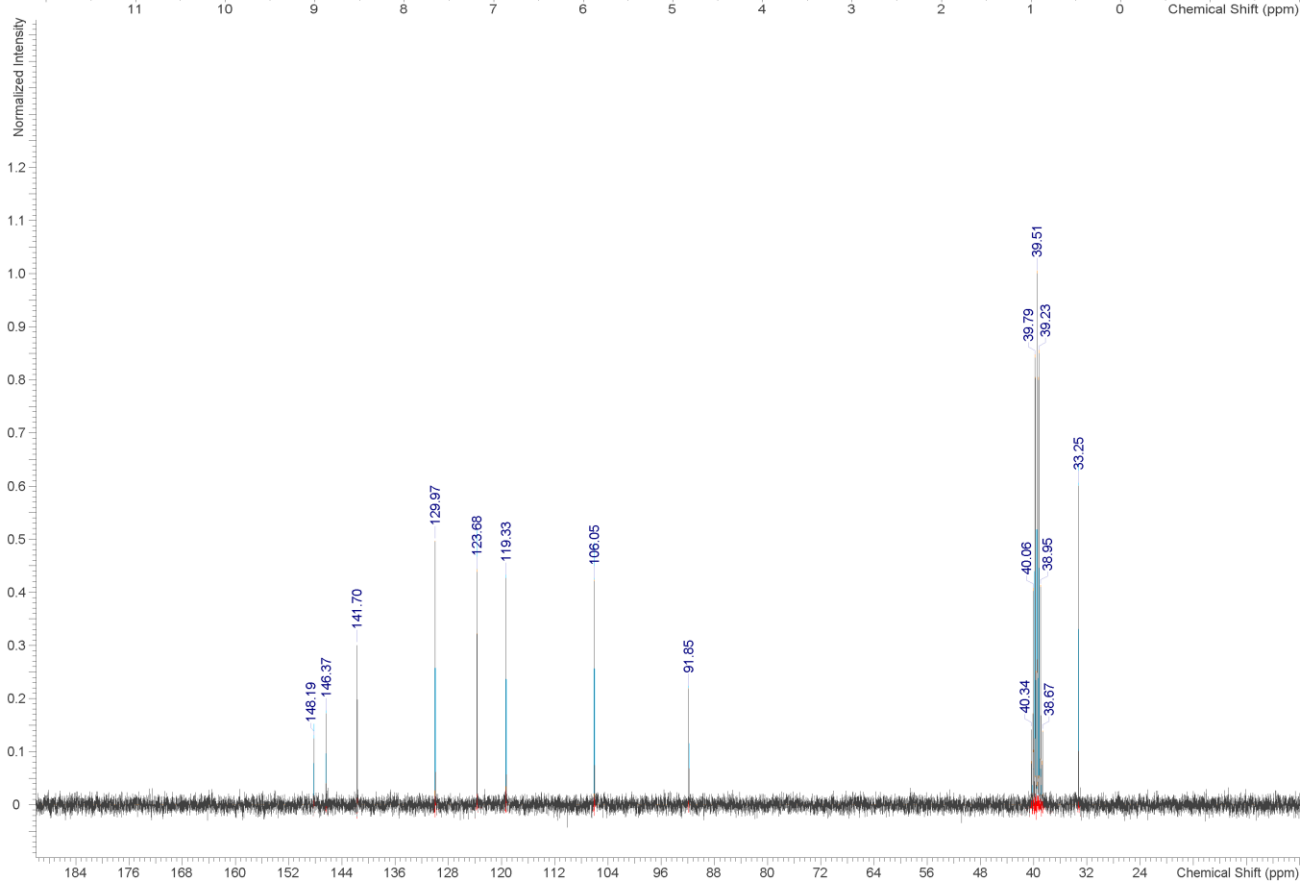

Top: ^{1}H-NMR (D_6-DMSO)

Bottom: ^{13}C-NMR (D_6-DMSO)

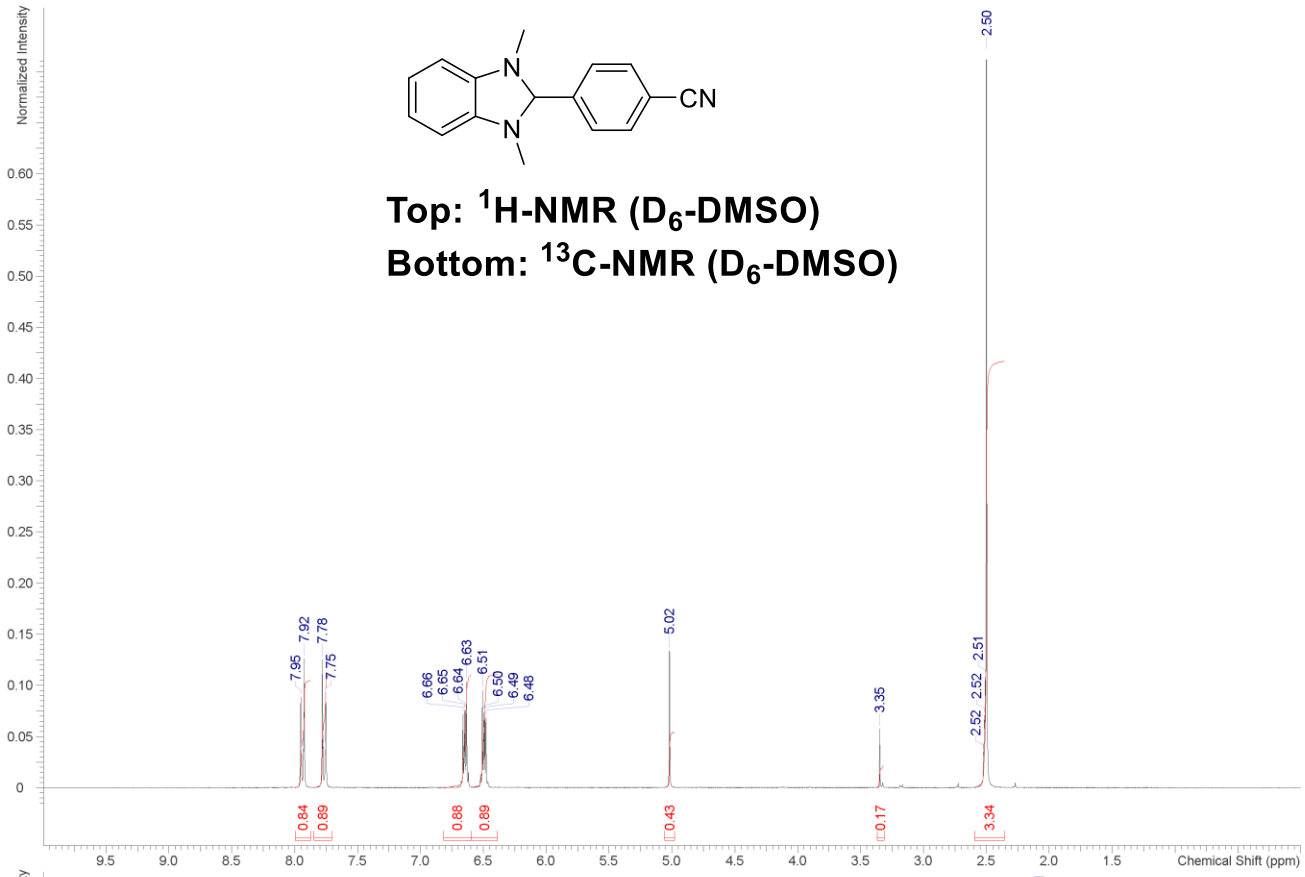
CN
N
N
Top: ^{1}H-NMR (D_6-DMSO)
Bottom: ^{13}C-NMR (D_6-DMSO)
Normalized Intensity
Chemical Shift (ppm)
2.50
7.95
7.92
7.78
7.75
6.66
6.65
6.64
6.63
6.51
6.50
6.49
6.48
5.02
3.35
2.52
2.51
0.84
0.89
0.88
0.89
0.43
0.17
3.34

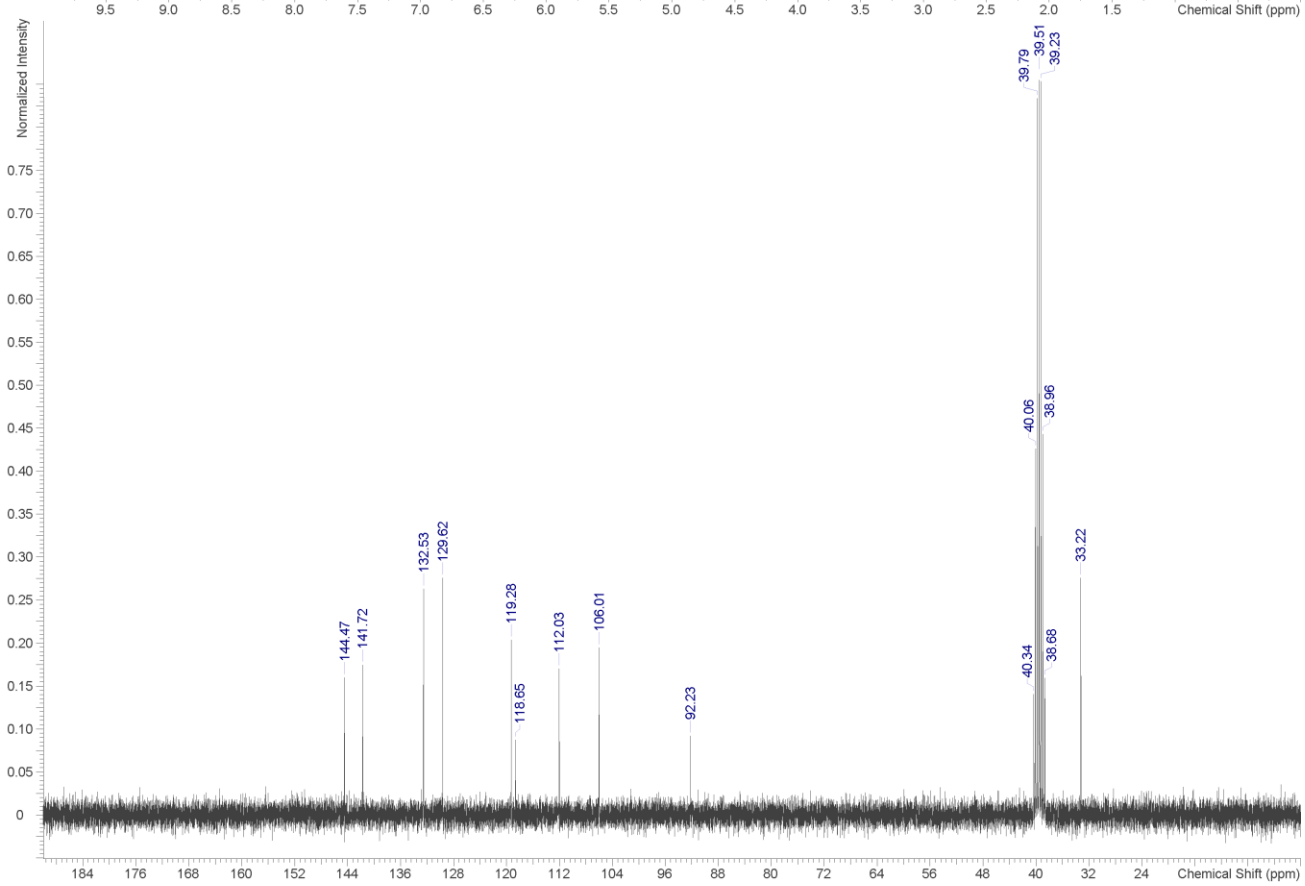
Normalized Intensity
Chemical Shift (ppm)
39.79
39.51
39.23
40.06
38.96
40.34
38.68
33.22
132.53
129.62
144.47
141.72
119.28
118.65
112.03
106.01
92.23